

AD-A278 716



AFOSR-TR- 94 0253

Approved for public release;
distribution unlimited.

**COMPUTATIONAL METHODS FOR MATERIAL
FAILURE PROCESSES**

2

Principal Investigator: Ted Belytschko

DTIC
S **ELECTE** **D**
APR 29 1994
F

FINAL REPORT
1 SEPTEMBER, 1990-31 DECEMBER, 1993

Air Force Research Grant
AFOSR-90-0340

This document has been approved
for public release and sale; its
distribution is unlimited.

Department of Civil Engineering
Robert McCormick School of Engineering and Applied Science
The Technological Institute
Northwestern University
Evanston, IL 60208-3109, U.S.A.

February 1994

DTIC QUALITY INSPECTED 3

94-12919



94 4 28 03 6

REPORT DOCUMENTATION PAGE

Form Approved
OMB No. 0704-0188

Public reporting burden for this collection of information is estimated to average 1 hour per response, including the time for reviewing instructions, searching existing data sources, gathering and maintaining the data needed, and completing and reviewing the collection of information. Send comments regarding this burden estimate or any other aspect of this collection of information, including suggestions for reducing this burden, to Washington Headquarters Services, Directorate for Information Operations and Reports, 1215 Jefferson Davis Highway, Suite 1204, Arlington, VA 22202-4302, and to the Office of Management and Budget, Paperwork Reduction Project (0704-0188), Washington, DC 20503.

1. AGENCY USE ONLY (Leave blank)		2. REPORT DATE February 1994		3. REPORT TYPE AND DATES COVERED Final: 1 Sept. 1990 to 31 Dec. 1993	
4. TITLE AND SUBTITLE Computational Methods for Material Failure Processes				5. FUNDING NUMBERS AFOSR-90-0340	
6. AUTHOR(S) Ted Belytschko					
7. PERFORMING ORGANIZATION NAME(S) AND ADDRESS(ES) Department of Civil Engineering Northwestern University Evanston, IL 60208				8. PERFORMING ORGANIZATION REPORT NUMBER AFOSR-TR- 94 0253	
9. SPONSORING / MONITORING AGENCY NAME(S) AND ADDRESS(ES) AFOSR NA 110 DUNCAN AVE SUITE B115 BOLLING AFB DC 20332-0001				10. SPONSORING / MONITORING AGENCY REPORT NUMBER	
11. SUPPLEMENTARY NOTES The view, opinions and/or findings contained in this report are those of the author(s) and should not be construed as an official Department of the Army position, policy, or decision, unless so designated by other documentation.					
12a. DISTRIBUTION AVAILABILITY STATEMENT Approved for public release; distribution unlimited.				12b. DISTRIBUTION CODE	
13. ABSTRACT (Maximum 200 words) Computational Methods are developed for failure problems such as shear banding. H-Adaptive procedures for the finite element solution of transient solid mechanics problems are studied, with particular emphasis on problems involving localization due to material instability. Various types of error criteria are examined and it is shown that for problems involving plastic response or localization, an error criterion based on an L2 projection of strains is the most effective for the constant strain elements considered here. Examples of one dimensional and two dimensional localization (shear band formation) problems are given. Massively parallel computations are performed to study the effects of imperfections on shear band morphology DTIC QUALITY INSPECTED 6					
14. SUBJECT TERMS Finite Elements, Material Instability Shear Bands				15. NUMBER OF PAGES 60	
				16. PRICE CODE	
17. SECURITY CLASSIFICATION OF REPORT UNCLASSIFIED	18. SECURITY CLASSIFICATION UNCLASSIFIED	19. SECURITY CLASSIFICATION OF ABSTRACT UNCLASSIFIED	20. LIMITATION OF ABSTRACT UL		

TABLE OF CONTENTS

PREFACE

i

CHAPTER 1 High Resolution Two Dimensional Shear Band Computations: Imperfections and Mesh Dependence

1.1. Introduction	1
1.2. Numerical Method	3
1.3. Numerical Solutions	7
1.4. Conclusions	11
Figures	18

CHAPTER 2 H-Adaptive Finite Element Methods for Dynamic Problems with Emphasis on Localization

2.1. Introduction	29
2.2. Governing Equations	31
2.3. Error Measures	33
2.4. Adaptive Procedure	36
2.5. Numerical Examples	38
2.6. Conclusions	43
Figures	51

Accession For	
NTIS	CRA&I
DTIC	TAB
Unannounced	
Justification	
By	
Distribution/	
Availability Codes	
Dist	Avail and/or Special
A-1	

PREFACE

The research was conducted under the direction of Professor Ted Belytschko. The following research personnel participated in the research program: Mr. Lee Bindeman, Mr. Mak Kulkarni and Mr. H.-Y. Chiang.

The following papers which were written under AFOSR support have been published during the course of the grant:

T. Belytschko, B. L. Wong and H.-Y. Chiang, "Advances in One-point Quadrature Shell Elements," *Computer Methods in Applied Mechanics and Engineering*, 96, pp. 93-107, 1992.

J. Donea and T. Belytschko, "Advances in Computational Mechanics," *Nuclear Engineering and Design*, 134, pp. 1-22, 1992.

T. Belytschko and N. D. Gilbertsen, "Implementtion of Mixed Time Integration Techniques on Vectorized Computer with Shared Memory," *International Journal for Numeridcal Methods in Engineering*, 35, pp. 1803-1828, 1992

T. Belytschko and Y. Y. Lu, "Convergence and Stability Anbalyses of Multi-Time Step Algorithm for Parabolic Systems," *Clmputer Methods in Applied Mechanics and Engineering*, 102, 2, pp. 179-198, 1993

T. Belytschko and L. P. Bindeman, "Asumed Strain Stabilization of the Eight Node Hexahedral Element," *Computer Methods in Applied Mechanics*, 105, pp. 225-260, 1993.

T. Belytschko and Y. Y. Lu, "Explicit Multi-time Step Integration for First and Second Order Finite Element Semidiscretizations," *Computer Methods in Applied Mechanics and Engineering*, 108, pp. 353-383, 1993.

The following personnel involved in the project during the past year were recipients of Ph.D.'s: Mr. Lee Bindeman and Mr. Mak Kulkarni.

Professor Ted Belytschko served in the following major offices during the past year:

President, U. S. Association for Computational Mechanics, 1992-94.

Chairman, First National Congress on Computational Mechanics, Chicago, July 1991.

Elected member of U. S. National Academy of Engineering, 1992.

Computational Mechanics Award, Japanese Society of Mechanical Engineers, 1993

CHAPTER 1

HIGH RESOLUTION TWO DIMENSIONAL SHEAR BAND COMPUTATIONS: IMPERFECTIONS AND MESH DEPENDENCE

1.1. INTRODUCTION

The calculation of shear bands and other material instability phenomena has become of considerable interest because of its importance in predicting material failure. This paper deals with two issues for this class of problems:

1. the role of imperfections in setting the length scale and structure of shear bands in two dimensional problems;
2. the behavior of various elements types for shear bands which are not aligned with element edges.

The primary tool used in examining these issues is a massively parallel version of an explicit program, Belytschko, Plaskacz, Kennedy, Greenwell (1990), and Belytschko, Plaskacz, Chiang (1991). By means of this program, we were able to solve problems using up to 64,000 elements.

For coarse meshes, numerical results are strongly mesh dependent for the shear band problem. Tvergaard *et al.* (1981) and Needleman and Tvergaard (1984) have used crossed-diagonal meshes of constant strain triangles and J_2 flow theory with strain-softening to calculate shear bands. The crossed-diagonal meshes developed by Nagtegaal, Parks and Rice (1974) were used to avoid volumetric locking. For these elements and the refinement which was used, it was necessary for the mesh to be arranged so that the diagonals of the mesh coincided with the orientation of the shear band. Otherwise, localization would not occur. This behavior of numerical solutions is often called mesh dependence.

Several approaches have been used to decrease mesh dependence for shear bands. Ortiz, Leroy and Needleman (1987) used the loss of ellipticity in an element to trigger the introduction of special step-function strain fields associated with incompatible modes of the quadrilateral element. Fish and Belytschko (1988) used embedded band-like functions triggered by loss of ellipticity to obtain good resolution with coarse meshes. Pietruszczak and Mroz (1981) first proposed a similar approach for triangular elements. However, these

approaches can only give improvement in the overall response of a body, such as the force-deflection curve. The detailed structure of the strain-field within the shear band, including the maximum strain, cannot be computed from these approaches.

Belytschko, Fish and Bayliss (1990) used a spectral overlay on finite elements, which was able to provide a detailed resolution in the shear band. They showed the critical role of the initial imperfection on the morphology of the strain field in the shear band. However, the method entailed *a priori* knowledge of the location of the shear band. Recently, an r-adaptive mesh refinement scheme has been applied to localization problems by Ortiz and Quigley (1991) and it proved quite effective, but detailed results on shear band structure were not given.

The critical issue of length scales in solutions of viscoplastic problems has perplexed numerous researchers. Quasi-static viscoplasticity, in the absence of heat conduction, lacks a length scale, and in dynamic problems the length scale is markedly smaller than the dimensions of shear bands. Several investigators, such as Pan (1983) and Shawki and Clifton (1989), have mentioned imperfections, but their critical role in determining the morphology of a shear band has not been studied extensively. Needleman (1988) demonstrated the role of imperfection size for stepwise imperfections in one-dimension. Belytschko, Bayliss and Fish (1990), by using a spectral overlay on finite elements which provided higher resolution at the shear bands, were able to show that the length and shape of an imperfection plays a critical role in determining the length scale of a shear band, as exhibited by its width. Subsequently, Belytschko, Moran and Kulkarni (1991) developed a closed-form solution for a class of one-dimensional viscoplastic problems which clearly demonstrated the dominant role of the imperfection in determining the shear band structure after the onset of material instability. They showed that the initial width of the shear band is completely determined by the initial width of the imperfection. Furthermore, they showed that step function imperfections, which are widely used in two-dimensional finite element calculations, are of questionable value insofar as the morphology of the shear band is concerned because these lead to unstable solutions. Batra and Liu (1990) have also studied the role of imperfections on adiabatic shear bands in two dimensions.

In this paper, dynamic formation and progression of two-dimensional shear bands is studied using much finer meshes than have previously been reported. Various sizes of imperfections are considered and both crossed-diagonal triangular element meshes and

quadrilateral meshes are used. It will be shown that the onset of localization and the structure of the shear band in the early stages of localization is independent of element type if the mesh is sufficiently refined compared to the scale of the imperfection. However, in a viscoplastic shear band the strain is characterized by an exponential growth which depends on the magnitude of the initial imperfection, so that the region of highest strain gradient narrows with time, and eventually only a few elements span this region. At this point, the solution becomes element and mesh-dependent.

It is also shown that in two dimensions, as in one dimension, the structure, location and size of the imperfection play a crucial role in the formation of the shear bands. For larger imperfections, the initial shear band is markedly wider, and in these large-scale computations often spans 6 to 10 elements. An interesting transition in the arrangement of shear bands was also noted in the computations: *when the size of the imperfection is reduced in one example, a transition to a set of parallel shear bands was noted.* Such transitions have also been observed in experiments.

The paper is organized as follows: Section 1.2 gives a brief outline of the computational method, Section 1.3 describes the computations and the results, and Section 4 gives some remarks and conclusions.

1.2. NUMERICAL METHOD

The problems were solved by a finite element method with a Lagrangian mesh. The rate-of-deformation tensor

$$\eta_{ij} = \frac{1}{2} \left(\frac{\partial v_i}{\partial x_j} + \frac{\partial v_j}{\partial x_i} \right) \quad \text{or} \quad \boldsymbol{\eta} = \mathbf{D} \mathbf{v} \quad (1)$$

is used as a measure of rate-of-deformation; here v_i are the velocities, x_i the Eulerian (spatial) coordinates.

The constitutive equation was expressed in terms of the Jaumann rate of Cauchy stress

$$\overset{\nabla}{\boldsymbol{\sigma}} = \mathbf{C} \boldsymbol{\eta} = \mathbf{C} \mathbf{D} \mathbf{v} \quad (2a)$$

$$\dot{\boldsymbol{\sigma}} = \overset{\nabla}{\boldsymbol{\sigma}} + \mathbf{w} \boldsymbol{\sigma} + \boldsymbol{\sigma} \mathbf{w}^T \quad (2b)$$

where $\dot{\sigma}$ is the Jaumann rate, C is a constitutive tangent matrix which depends on the current state of stress, and w is the spin tensor.

The governing equations are Eqs. (1) and (2) and the momentum equation

$$\sigma_{ij,j} + b_i = \rho \dot{v}_i \quad \text{or} \quad D^T \sigma + b = \rho \dot{v} \quad (3)$$

In two dimensions, Eqs. (1-3) represent 5 equations in the 5 unknowns s_{ij} and v_i .

The finite element equations are obtained by approximating the velocities in each element by

$$v(X,t) = N(X) \dot{d}_e(t) \quad (4)$$

The resulting ordinary differential equations are:

momentum equation

$$M \mathbf{a}(t) = \mathbf{f}(t) \quad \mathbf{a} = \frac{D^2 \mathbf{d}}{Dt^2} = \ddot{\mathbf{d}}(t) \quad (5)$$

$$\mathbf{f}(t) = \mathbf{f}_{ext}(t) - \mathbf{f}_{int}(t) \quad (6)$$

$$\mathbf{f}_{ext} = \sum_e \mathbf{L}_e^T \mathbf{f}_{ext}^e(t) \quad \mathbf{f}_{int} = \sum_e \mathbf{L}_e^T \mathbf{f}_{int}^e(t) \quad (7)$$

$$\mathbf{f}_{int}^e(t) = \int_{\Omega_e} \mathbf{B}^T \sigma d\Omega \quad (8)$$

measure of rate-of-deformation

$$\eta(X,t) = \mathbf{B}(X) \dot{\mathbf{d}}_e(t) \quad \mathbf{B} = \mathbf{D} \mathbf{N} \quad (9)$$

$$\dot{\mathbf{d}}_e(t) = \mathbf{L}_e \mathbf{d}(t) \quad (10)$$

and the constitutive equation (2). In the above

t = time;

M = mass matrix;

\mathbf{d} = nodal displacement matrix;

\mathbf{X} = material coordinate;

$\mathbf{f}(t)$, $\mathbf{f}_{\text{ext}}(t)$, $\mathbf{f}_{\text{int}}(t)$ = resultant, external and internal nodal forces, respectively;

$\mathbf{B}(\mathbf{X})$ = semidiscrete form of the symmetric part of the gradient operator;

$\boldsymbol{\eta}$ = rate-of-deformation (velocity strain) tensor;

\mathbf{L}_e = Boolean connectivity matrix of element e .

The SIMD algorithm is described in Belytschko, Plaskacz, Kennedy and Greenwell (1990). The algorithm uses an exchange of forces at each time step and integrates the nodes redundantly so that only one communication is required in each time step, in contrast to the two communications required in a standard gather-scatter finite element algorithm. The exchange algorithm can also be used to advantage in MIMD computers. The essential idea here is to use the gather-scatter operations within each subdomain, so that gather-scatter does not require communication between processors. The exchange operation is then used to communicate nodal forces for the interface nodes to the adjacent subdomains. Note that the interfaces nodes are integrated redundantly by all processors which contain elements connected to those nodes. However, this extra cost is compensated by the reduction in communication costs brought about by the fact that communication is required only once per time step. The algorithm for a MIMD implementation is shown in Table 1.

Table 1. MIMD implementation of exchange algorithm

```
loop over subdomains I (processors)
  loop over elements e in subdomain I

    gather nodal velocity  $\mathbf{v}_e$ 
    compute rate-of-deformation by Eq.(9)
    compute stress by constitutive equation
    compute nodal forces  $\mathbf{f}^e$ 
    assemble nodal forces
```

```

        end loop on e
    end loop on I

    exchange forces on interface nodes between subdomains

    compute accelerations by Eq. (5)

    integrate to obtain new velocities and displacements

```

Incidentally, this algorithm was not very effective on the CM5, probably because of inefficiencies in user-directed message passing. However, on the DELTA this algorithm proved quite efficient.

The equations were integrated in time by the explicit central-difference method. Two types of elements were used in these computations:

1. Quadrilaterals with one-point quadrature and consistent hourglass control (Flanagan and Belytschko(1981)), with a perturbation stabilization parameter $\epsilon = 0.01$.
2. Constant strain triangles arranged in the crossed-diagonal pattern which avoids volumetric locking, Nagtegaal, Parks and Rice(1974).

A viscoplastic stress-strain law in which

$$\dot{\sigma} = C^{elas}(\dot{\eta} - \dot{\eta}^{vp}) \quad (11)$$

was used; C^{elas} is the elastic constitutive matrix and $\dot{\eta}^{vp}$ the viscoplastic strain rate.

The von Mises yield surface has been used to determine the flow direction and the rate of viscoplastic strain can be defined as follows

$$\dot{\eta}_{ij}^{vp} = \bar{\eta}(\bar{\sigma}, \bar{\epsilon}) \frac{\partial f}{\partial \sigma_{ij}} \quad (12a)$$

$$f(\sigma, k) = \bar{\sigma} - k = 0 \quad (12b)$$

where effective stress $\bar{\sigma}$ and effective viscoplastic strain $\bar{\epsilon}$ are given by

$$\bar{\sigma}^2 = \frac{3}{2} \mathbf{s} : \mathbf{s} \quad (13)$$

where \mathbf{s} is the deviatoric stress and

$$\bar{\epsilon} = \int_0^t \sqrt{\frac{2}{3} \dot{\eta}^{vp} : \dot{\eta}^{vp}} dt \quad (14)$$

and the power law used here to determine the rate of effective viscoplastic strain is

$$\bar{\eta} = \alpha \left[\frac{\bar{\sigma}}{g(\bar{\epsilon})} \right]^{1/m} \quad (15)$$

where α and m are material properties and $g(\bar{\epsilon})$ is the hardening function.

The rate tangent modulus scheme, see Peirce, Shih and Needleman (1984), is used for the constitutive update for each time step, so the viscoplastic strain is updated as follows:

$$\Delta \bar{\epsilon} = \Delta t [(1 - \theta) \dot{\bar{\epsilon}}_t + \theta \dot{\bar{\epsilon}}_{t+\Delta t}] \quad (16)$$

where the parameter θ can vary from 0 to 1; the $\theta = 0$ and $\theta = 1$ are the forward and backward Euler method, respectively. We choose $\theta = 0.5$ here, which corresponds to a semi-implicit central difference update. To maintain accuracy in the later stages of localization, the time step should be decreased, because the exponential growth of the strains in the band can lead to significant truncation errors.

1.3. NUMERICAL SOLUTIONS

Calculations were performed for a square slab in plane strain as shown in Fig. 1. A velocity was prescribed at the ends as shown: after a ramp, the constant value v_0 is 30.0 m/sec. The problem specification is shown in Fig. 1; it is similar to Needleman (1989). Most of the calculations were made on a CM200.

In all cases, an initial imperfection was included in the form of a reduction in the yield strength. One of the imperfections is

$$\sigma_Y(x,y) = \bar{\sigma}_Y [1 - \alpha \exp\{-(x - x_0)^2 - (y - y_0)^2\} / r_0^2] \quad (17)$$

where x_0 , y_0 specify the location of the maximum imperfection and r_0 its radius. In the problems reported here, $x_0 = y_0 = 0$ except where noted and $a = 0.20$. The same viscoplastic material law as reported by Needleman (1989) was used: Young's modulus $E = 211$ GPa, $\bar{\sigma}_Y = 460$ MPa, Poisson's ratio $\nu = 0.3$, the viscoplastic exponent $m = 0.01$.

In the first example, two planes of symmetry were used and only the upper right-hand quadrant was modeled. Unless noted, a value r_0 of 0.1 mm was used; this will be called the large imperfection. A deformed 26×20 quadrilateral element mesh is shown in Fig. 3a and exhibits no localization; Needleman obtained shear banding by using a similar refinement in a crossed-triangular mesh and aligning the diagonal of quadrilateral elements with the expected direction of shear band. The results we have obtained for the crossed-triangular mesh, shown in Fig. 3b, also show localization. Note that most of the deformation occurs in a single band, so the width of the shear band is only slightly larger than the element size. This is a consequence of the fact that the effective size of the imperfection is of the order of the element size. In these results, the strain field is a step function in space since the elements are constant strain elements and one or two elements span the entire shear band.

The same problem was then solved with a 128×128 mesh, i.e. 16K equally sized elements. Twofold symmetry was again used in this problem, so only the upper right-hand quadrant is modeled. The evolution of the mesh for the upper right-hand quadrant is shown in Figs. 4 through 6. The figures show the development of a shear band approximately 10 elements in width. Figs. 7 and 8 show contour plots of the effective viscoplastic strain, from which it can be seen that the deviation from uniform strain first occurs over a band of 8 to 10 elements. The structure of the strain field varies somewhat along the length of the band initially, but becomes quite uniform in the later stages, except at the two points where the shear bands intersect (at the center of the plate and at the top surface). With time, the region of largest strain narrows. Figure 9 shows the deformed mesh for the same problem with a 80×80 mesh. As can be seen by comparison with Fig. 4, the deformed meshes almost appear identical.

Figure 10 shows the profiles of the effective viscoplastic strain, given by Eq.1.14, across the shear band; this quantity gives a good measure of the severity of deformation. Results are also shown for when: (1) each quadrilateral element is replaced by 4 constant strain triangular elements in a cross-diagonal pattern, so the total number of elements is 64K; (2) quadrilaterals using selective-reduced integration are used. The plots were made

using the effective viscoplastic strains in the elements which lie along the line $Y = 1.0 + aX$, where a is chosen so the line is perpendicular to the direction of shear band. It can be seen that the effective plastic strain profiles for the different elements are almost identical for $t = 2.0\mu\text{sec}$ and for $t = 3.0\mu\text{sec}$. At later times, a significant difference develops, and the maximum effective strain differs markedly for the three different elements. However, it should be noted that the growth of the strain is exponential just as in the one dimensional problem; see Belytschko, Moran and Kulkarni(1991) for a one-dimensional solution. As a consequence, the strain-rate increases with the strain and grows most rapidly at the point where it is maximum. Therefore, the band appears to narrow in time and the highest gradients occur at the center, where the strain profile becomes cusp-shaped. At $4.0\mu\text{sec}$, the cusp-shaped region has narrowed to 1 or 3 elements. The resolution in the cusp-shaped region is then insufficient, and the peak strain becomes very dependent on the type of element. Thus, inevitably, after a sufficiently long time, these meshes becomes inadequate for the viscoplastic strain-softening problem.

The problem was repeated with an 80×80 mesh using the same stabilization parameters ($\epsilon = 0.01$) and a larger stabilization parameter ($\epsilon = 0.05$). The strain profiles are shown in Fig. 11. Comparison of the results with $\epsilon = 0.01$ to those for the 128×128 mesh (top of Fig. 10) shows that the strain profiles for $t = 2.0\mu\text{sec}$ and for $t = 3.0\mu\text{sec}$ agree closely. Similarly, for the two values of the stabilization parameter the first two results are almost identical. However, the result at $t = 4.0\mu\text{sec}$ differs markedly. This marked difference is also attributed to insufficient resolution when the cusp-shaped region only spans a few elements.

The load deflection curves for meshes of different size using the one-point quadrature element with stabilization are compared in Fig. 12. It can be seen that the results are almost identical for the three meshes until the latest stage of the deformation; the horizontal axis after $t = 1.0\mu\text{sec}$ corresponds to time because the velocity is constant. The load deflection curves for the one-point quadrature element with stabilization (URI), the constant strain triangles in the cross-diagonal pattern and the SRI element are compared in Fig. 13. These results are also almost identical except for the later stages; it is interesting to note that the results for the triangular element and the URI element are almost identical throughout the simulation.

The problem was repeated with a 128×128 quadrilateral mesh with the imperfection of Eq. 1.17 with $\alpha = 0.20$, $r_0 = 0.0039\text{mm}$, i.e. a smaller imperfection. The deformed

mesh is shown in Fig. 14, the effective viscoplastic strain profile in Fig. 15. The change in the response (as compared to Figs. 7 and 8) is quite dramatic: the reduction of the size of the imperfection *reduces the width of the shear band and introduces 4 additional intersecting shear bands in the quadrant*. Apparently, with the smaller imperfection, the deformation due to the shear band through the imperfection is not sufficient to accommodate the prescribed displacement of the top surface and additional shear bands are triggered. This phenomenon has also been observed experimentally, Anand, Kim and Shawki(1987).

A much smaller imperfection, $r_0 = 0.00195\text{mm}$, was also used for the same problem. Again, an interesting result was found. Although the shear band pattern is the same as in the previous results, the larger viscoplastic strains now occur in the shear bands which do not pass through the imperfection; see the contour plots of the effective viscoplastic strain, Fig. 16. This result again shows the crucial role of imperfections in the structure of the shear bands.

To further assess the effects of the size of the imperfection, the results were repeated with the imperfections:

$$\begin{aligned}\sigma_Y(x,y) &= \bar{\sigma}_Y \{0.9 + 0.01[(x - x_0)^2 - (y - y_0)^2] / r_0^2\} & r < r_0 \\ &= \bar{\sigma}_Y & r \geq r_0\end{aligned}\quad (18)$$

with $r_0=0.078\text{mm}$ and $r_0=0.156\text{mm}$; these correspond to 10 and 20 elements, respectively. The effective viscoplastic strain profiles at $4.0\mu\text{sec}$ are given in Fig. 17. It can be seen that the width of the shear band is approximately twice as great for $r_0 = 0.156\text{mm}$. It is interesting to note that the peak strain is equal for these two cases at $t = 4.0\mu\text{sec}$; it is evidently set by the maximum magnitude of the imperfection, which in this case is identical. The maximum magnitude of the imperfection is smaller than for the calculation shown in Fig. 10, and so the maximum strain is lower.

The location of the imperfection also plays an important role in the shear band pattern. Figure 18 shows the shear band pattern in the upper half of the plate when an imperfection given by Eq.17 with $\alpha = 0.2$ and $r_0=0.10\text{mm}$ is placed at $x_0 = -0.25\text{mm}$, $y_0=0.0\text{mm}$. The shear band pattern now loses symmetry with respect to the x -plane in order to pass through the imperfection. Similar patterns are observed when the

imperfection is placed anywhere on the $y=0.0$ axis. However, when an imperfection is not placed along the centerline, no shear bands are observed in the computation for a long time (our computations were of course limited in duration). For example, when the imperfection of Eq.(17) was placed at $x=0.1\text{mm}$, $y=1.0\text{mm}$ no shear band pattern was triggered during the first $4.0\mu\text{sec}$. Thus, the appearance and structure of the shear band in these dynamic problems depends on an interplay between wave focusing and the position of the imperfection.

1.4. CONCLUSIONS

The results we have obtained show the following:

1. imperfections play an important role in the setting the external and internal structure of shear bands in viscoplastic materials and can be said to set a length scale for viscoplastic materials in that the dimensions of the imperfection set the initial width and structure of the shear band;
2. little difference is found in the results obtained with different elements or different values of the stabilization parameter as long as the mesh is sufficiently refined so that more than five elements occur within the high gradient region of the shear band.

For coarse meshes, quadrilateral elements tend to exhibit less of a tendency to bifurcate than cross-diagonal triangular meshes; this was also noted by Ortiz, Leroy and Needleman(1987) and Belytschko, Fish and Englemann(1988). It has been shown here that for meshes in which the elements are small compared to the scale of the imperfection, mesh-dependence for the onset and early stages of localization behavior is insignificant. The results obtained here show that quadrilaterals with different quadrature schemes and triangular elements give similar solutions as long as the mesh is sufficiently fine to capture the high strain gradients in the center of the band. Even for the finest meshes used here, this condition is met only for about $3\mu\text{sec}$, which correspond to the early stages of localization.

However, in the uncoupled viscoplastic localization, the strain profiles develop a cusp-shaped profile which narrows with time. When the cusp becomes narrow enough relative to element size, the resolution is insufficient and the maximum effective strain and the structure of the band start to depend markedly on the type of element, mesh refinement and stabilization procedure. It should be stressed that this mesh dependence is strictly a

consequence of lack of resolution. To obtain reasonable accuracy, the portion of the shear band in which the strain changes most rapidly must be spanned by 4 to 7 constant strain elements (just as an elastic wave in a finite element mesh must be spanned by 4 to 7 elements for reasonable accuracy). Since the high gradient part of the cusp narrows with time, any fixed mesh will eventually prove inadequate. Thus, there is no evidence of any pathological mesh dependence in these results. If the region of highest strain gradient is covered by only one or two elements, the well known manifestations of truncation error appear.

The running time for the uniform 16K mesh in these explicit calculations is about 1.4 μ sec for each element cycle on the CM200. The crossed-triangular fine mesh requires about 7 times as much wall clock time as the quadrilateral mesh. We would expect an increase of only a factor of 4, but evidently the increased memory requirements of crossed-triangular meshes reduce the speed further.

The location and size of the imperfection have been shown to play a critical role in both the internal shear band structure and the arrangement and multiplicity of shear bands. By reducing the size of the imperfection, an interesting transition to multiple shear bands was noted. This appears to arise from the interplay of strain concentrations caused by the wave motion and the effect of the imperfection. Such multiple shear bands have been noted in experiments by Anand et al. (1987). The major role of imperfections in setting the internal morphology of shear bands has also been demonstrated in a two dimensional, dynamic problem. In previous studies, because of computer limitations, two dimensional meshes usually used elements of the same size as the imperfection, so the importance of the imperfection could not be observed.

REFERENCES

- Anand, L., Kim, K.H. and Shawki, T.G.(1987), Onset of Shear Localization in Viscoplastic Solids, *J. Mech. Phys. Solids*, **35**, 407.
- Batra, R.C. and Liu (1990) *International Journal of Plasticity*
- Belytschko, T., Chiang, H-Y and Plaskacz E.(1992), Two-Dimensional Shear Band Computations and The Effects of Imperfection, Proceedings of 3rd International Conference on Computational Plasticity, Barcelona, April 6-10, 1992.
- Belytschko, T., Fish, J. and Bayliss, A.(1990), The Spectral Overlay on Finite Elements for Problems With High Gradients, *Comp. Meths. Appl. Mech. Engrg.*, **81**, 71-89.
- Belytschko, T., Fish, J. and Englemann, B.(1988), A Finite Element Method with Embedded Localization Zones, *Comp. Meths. Appl. Mech. Engrg.*, **70**, 59-90.
- Belytschko, T., Moran, B. and Kulkarni, M.(1991), On the Crucial Role of Imperfections in Quasi-static Viscoplastic Solutions, *J. Appl. Mech.*, **58**, 658-665.
- Belytschko, T., Plaskacz, E. and Chiang, H-Y(1991), Explicit Finite Element Methods With Contact-Impact on SIMD Computers, *Comp. Sys. in Engrg.*, **2(2/3)**, 269-276.
- Belytschko, T., Plaskacz, E., Kennedy, J. and Greenwell, D.L.(1990), Finite Element Analysis on the CONNECTION Machine, *Comp. Meths. Appl. Mech. Engrg.*, **81(2)**, 229-254.
- Fish, J. and Belytschko, T.(1988), Elements with Embedded Localization Zones for Large Deformation Problems, *Comp. Struc.*, **30**, 247.
- Flanagan, D. P. and Belytschko, T.(1981), A Uniform Strain Hexahedron and Quadrilateral with Orthogonal Hourglass Control, *Int'l J. Num. Meths. Engrg.*, **17**, 679-706.
- Hill, R.(1962), Acceleration waves in solids, *J. Mech. Phys. Solids*, **10**, 1-16.

- Nagtegaal, J. C., Parks, D. M. and Rice, J. R.(1974), On Numerically Accurate Finite Element Solutions in The Plastic Range, *Comp. Meths. Appl. Mech. Engrg.*, **4**(2), 153-177.
- Needleman, A. and Ortiz, M.(1991), Effect of Boundaries and Interfaces on Shear-Band Localization, *Int'l. J. Solids Struct.*, **28** (7), 859-877.
- Needleman, A. and Tvergaard, V.(1992), Analysis of Plastic Flow Localization in Metals, *Appl. Mech. Rev.*, **45**(3/2), S3-S18.
- Needleman, A.(1989), Dynamic Shear Band Development in Plane Strain, *J. Appl. Mech.*, **56**, 1-9.
- Needleman, A.(1988), Material Rate Dependence and Mesh Sensitivity in Localization Problem, *Comp. Meths. Appl. Mech. Engrg.*, **67**, 69-85.
- Ortiz, M., Leroy, Y. and Needleman, A.(1987), A Finite Element Method for Localized Failure Analysis, *Comp. Meths. Appl. Mech. Engrg.*, **61**,189-214.
- Ortiz, M. and Quigley, J.J. IV(1991), Adaptive Mesh Refinement in Strain Localization Problem, *Comp. Meths. Appl. Mech. Engrg.*, **90**, 781-804.
- Pan, J.(1983), Perturbation Analysis of Shear Strain Localization in Rate Sensitive Materials, *Int'l. J. Solids and Struct.*, **19**, 153-164.
- Pan, J., Saje, M. and Needleman, A.(1983), Localization of Deformation in Rate Sensitive Porous Plastic Solids, *Int'l. J. of Fracture*, **21**, 261-278.
- Peirce, D., Shih, C. F. and Needleman, A.(1984), A Tangent Modulus Method For Rate Dependent Solids, *Comp. Struct.*, **18**(5), 875-887.
- Pietruszczak, S. and Mroz, A.(1981), Finite Element Analysis of Deformation of Strain-Softening Materials, *Int'l J. Num. Meths. Engrg.*, **17**, 327-334.
- Rice, J.(1977), The Localization of Plastic Deformation, Theoretical and Applied Mechanics, in Koiter W.T., ed., Proceedings 14th International Congress on Theoretical and Applied Mechanics (North-Holland, Amsterdam.), 207-220.

Shawki, T. G., Sherif R. A. and Cherukuri, H. P.(1992), Characterization of The Flow Localization History in Dynamic Viscoplasticity, *Appl. Mech. Rev.*, **45(3/2)**, S149-S153.

Shawki, T. G. and Clifton, R. J.(1989), Shear Band Formation in Thermal Viscoplastic Materials, *Mech. of Mat'l.*, **8**, 13-43.

Shawki, T. G.(1992), The Phenomenon of Shear Strain Localization in Dynamic Viscoplasticity, *Appl. Mech. Rev.*, **45(3/2)**, S46-S61.

Tvergaard, V., Needleman, A. and Lo, K. K.(1981), Flow Localization in the Plane Strain Tensile Test, *J. Mech. Phys. Solids*, **29**, 115-142.

Captions

Fig. 1.1. Description of model problem

Fig. 1.2. Stress-strain functions for examples; note strain-softening after effective plastic strain $\bar{\epsilon}$ is about 0.1

Fig. 1.3a. Deformed mesh at 6.0 μsec with quadrilateral elements; $r_0 = 0.1\text{mm}$

Fig. 1.3b. Deformed mesh at 6.0 μsec with crossed-triangular elements (only quadrilaterals are shown); $r_0 = 0.1\text{mm}$.

Fig. 1.4. Deformed mesh for 128x128 quadrilateral elements with $\alpha=0.2$ at $t = 4.79\mu\text{sec}$.

Fig. 1.5. Deformed mesh for 128x128 quadrilateral elements with $\alpha=0.2$ at $t = 6.00\mu\text{sec}$.

Fig. 1.6. Deformed mesh for 128x128 quadrilateral elements with $\alpha=0.2$ at $t = 7.25\mu\text{sec}$.

Fig. 1.7. Effective viscoplastic strain in the problem of Fig. 4 through 6 at $t = 4.0\mu\text{sec}$; 128x128 quadrilateral mesh, $r_0 = 0.1\text{mm}$.

Fig. 1.8. Effective viscoplastic strain in the problem of Fig. 4 through 6 at $t = 7.25\mu\text{sec}$; 128x128 quadrilateral mesh, $r_0 = 0.1\text{mm}$.

Fig. 1.9. Deformed mesh for 80x80 quadrilateral elements with $\alpha=0.2$ at $t = 4.79 \mu\text{sec}$.

Fig.1.10. Effective viscoplastic strain profiles across the shear band for quadrilaterals(top), the 128x128 crossed-diagonal triangular element mesh (middle) and quadrilaterals with selective-reduced integration SRI (bottom) at $t=2.0, 3.0, 4.0 \mu\text{sec}$, respectively, $r_0 = 0.1\text{mm}$; all meshes are 128x128.

Fig.1.11. Effective viscoplastic strain profiles across the shear band for quadrilateral 80x80 with stabilization parameters of 0.01 (top) and 0.05 (middle).

Fig.1.12. Average stress versus end displacement curves for three types of elements in a 128x128 mesh: constant strain triangles, quadrilaterals with selective reduced integration (SRI) and quadrilaterals with one-point underintegration and stabilization(URI).

Fig. 1.13. Average stress versus end displacement curves for three meshes of one-point quadrature elements; 6,400 elements, 10,000 elements and 16,384 elements.

Fig.1.14. Deformed mesh for small imperfection, $r_0=0.0039\text{mm}$, at $t=7.25\text{ }\mu\text{sec}$, showing of multiple shear bands.

Fig.1.15. Effective viscoplastic strain for small imperfection at $t=7.25\text{ }\mu\text{sec}$; $r_0=0.0039\text{mm}$.

Fig.1.16. Effective viscoplastic strain across the shear band for small imperfection at $t=7.25\text{ }\mu\text{sec}$ ($r_0=0.00195\text{mm}$) showing the development of multiple shear bands with markedly different strain distributions than in Fig. 1.15.

Fig.1.17. Effective viscoplastic strain profiles across the band for the imperfection Eq.(18) at $t=4.0\mu\text{sec}$.

Fig 1.18. Deformed mesh for upper *half* of specimen at $t=5.0\mu\text{sec}$ for imperfection at $x=-0.25\text{mm}$, $y=0.0$; $r_0=0.1\text{mm}$.

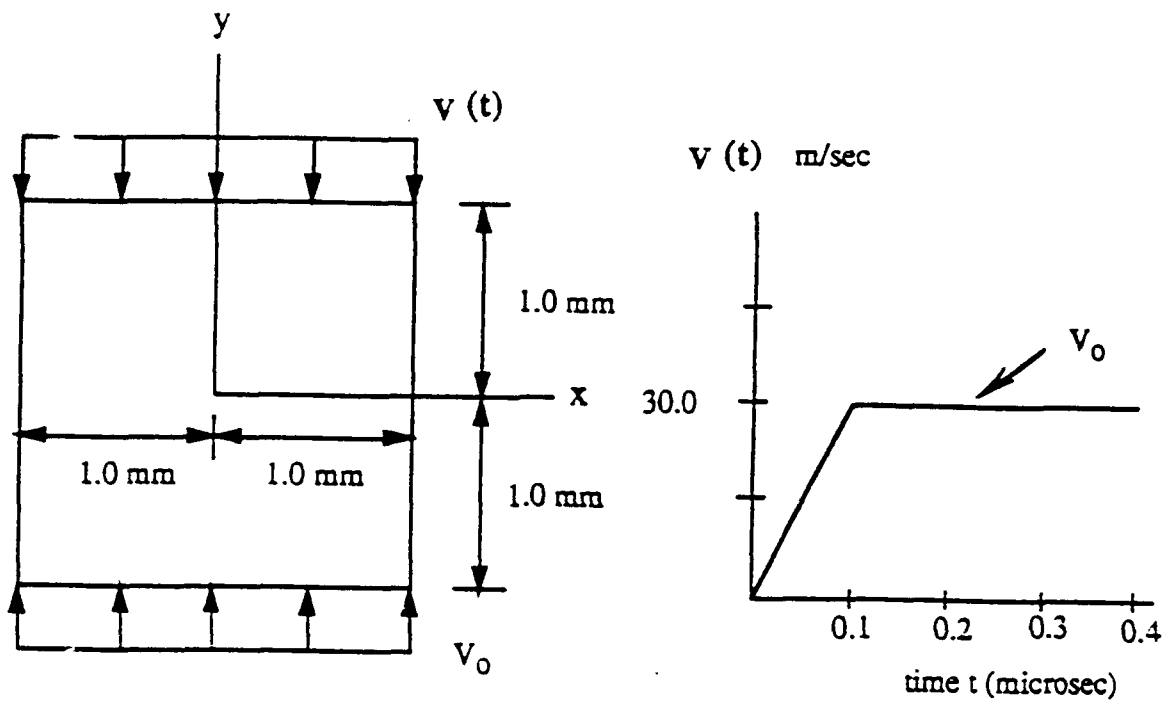


Fig. 1.1. Description of model problem

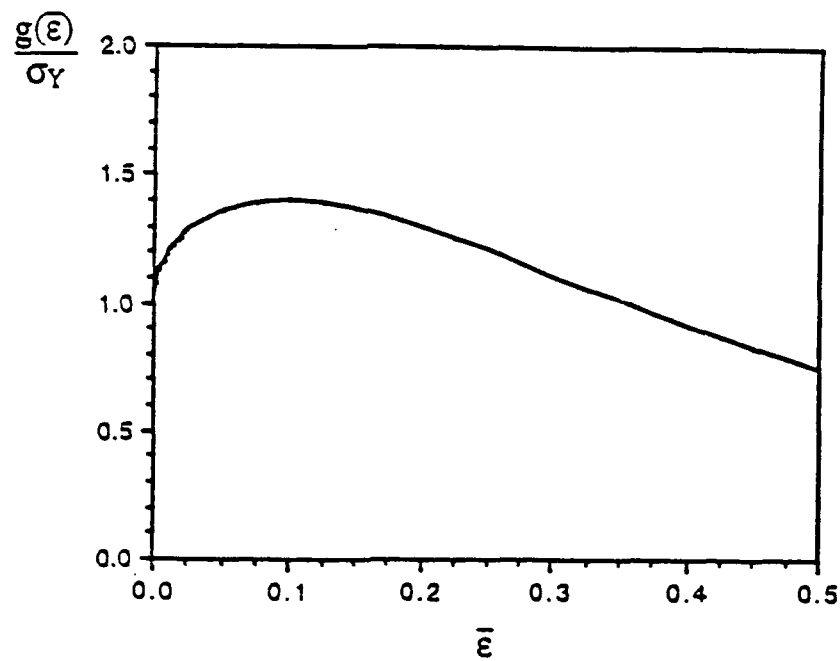


Fig. 1.2. Stress-strain functions for examples; note strain-softening after effective plastic strain $\bar{\epsilon}$ is about 0.1

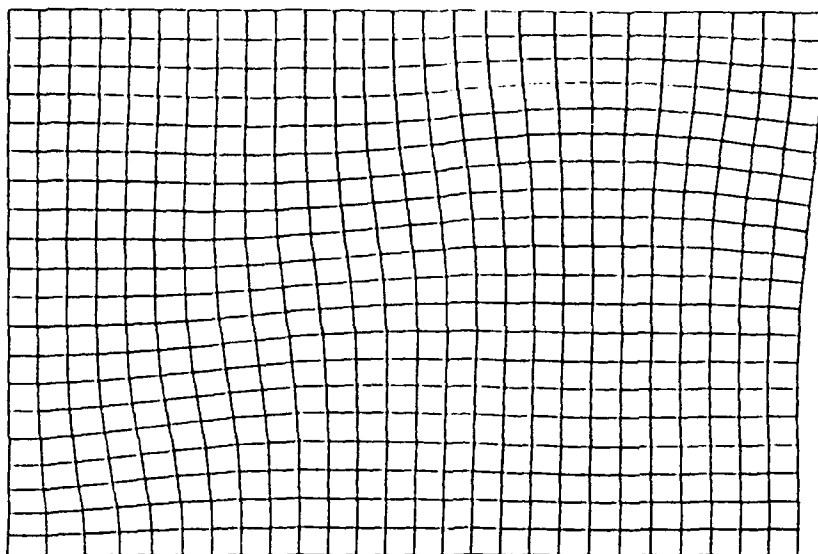


Fig. 1.3a. Deformed mesh at $6.0 \mu\text{sec}$ with quadrilateral elements; $r_0 = 0.1\text{mm}$

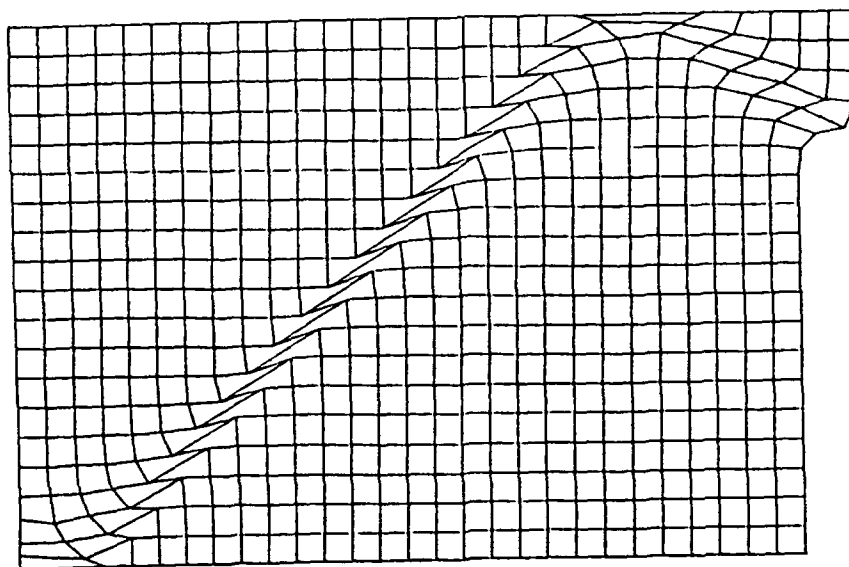


Fig. 1.3b. Deformed mesh at $6.0 \mu\text{sec}$ with crossed-triangular elements (only quadrilaterals are shown); $r_0 = 0.1\text{mm}$.

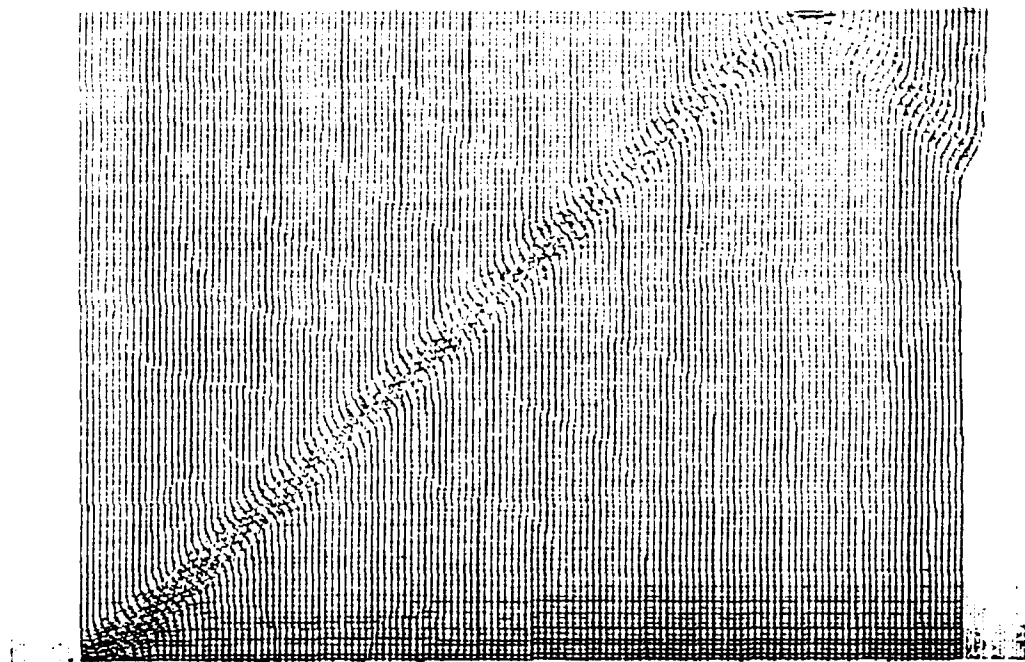


Fig. 1.4. Deformed mesh for 128x128 quadrilateral elements with $\alpha=0.2$ at $t = 4.79\mu\text{sec}$.

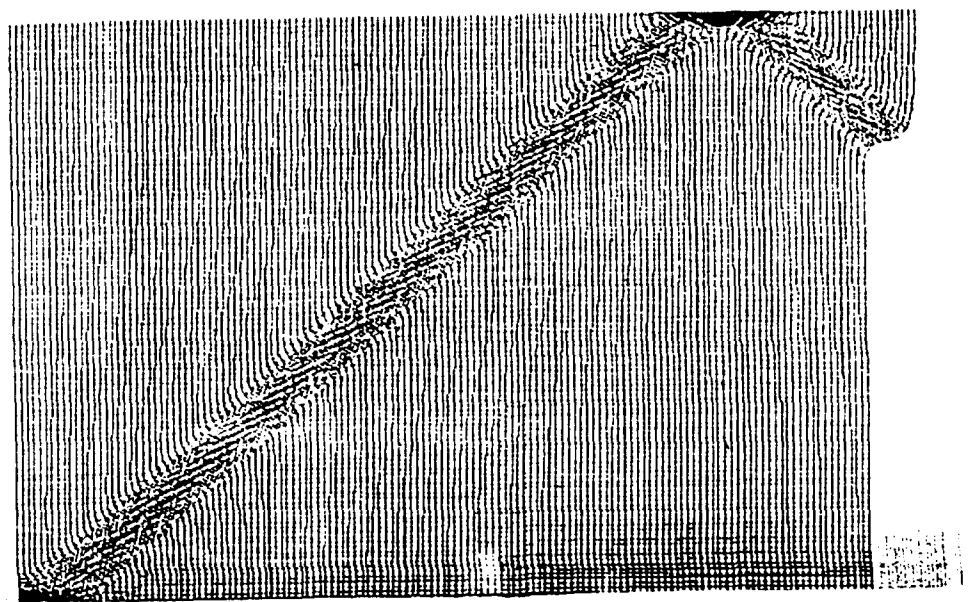


Fig. 1.5. Deformed mesh for 128x128 quadrilateral elements with $\alpha=0.2$ at $t = 6.00\mu\text{sec}$.

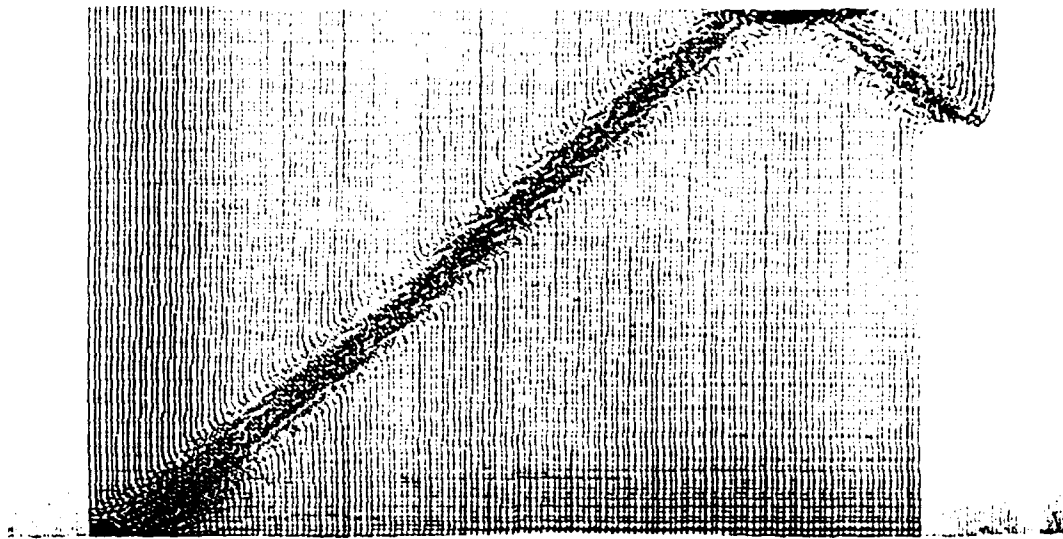


Fig. 1.6. Deformed mesh for 128×128 quadrilateral elements with $\alpha=0.2$ at $t = 7.25 \mu\text{sec}$.

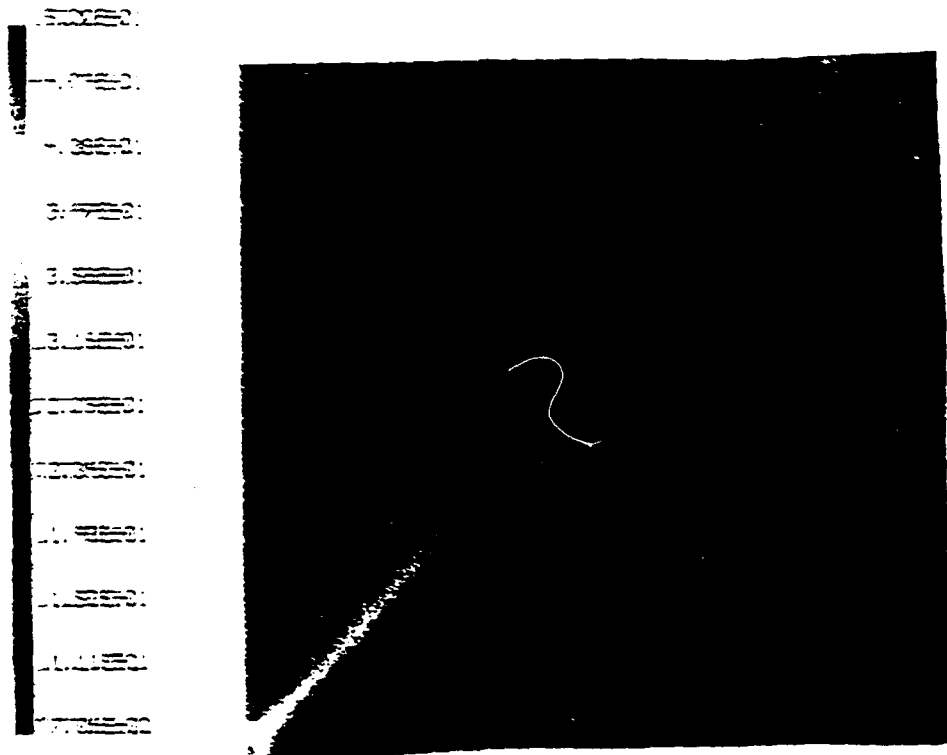


Fig. 1.7. Effective viscoplastic strain in the problem of Fig. 4 through 6 at $t = 4.0 \mu\text{sec}$; 128×128 quadrilateral mesh, $r_0 = 0.1 \text{ mm}$.

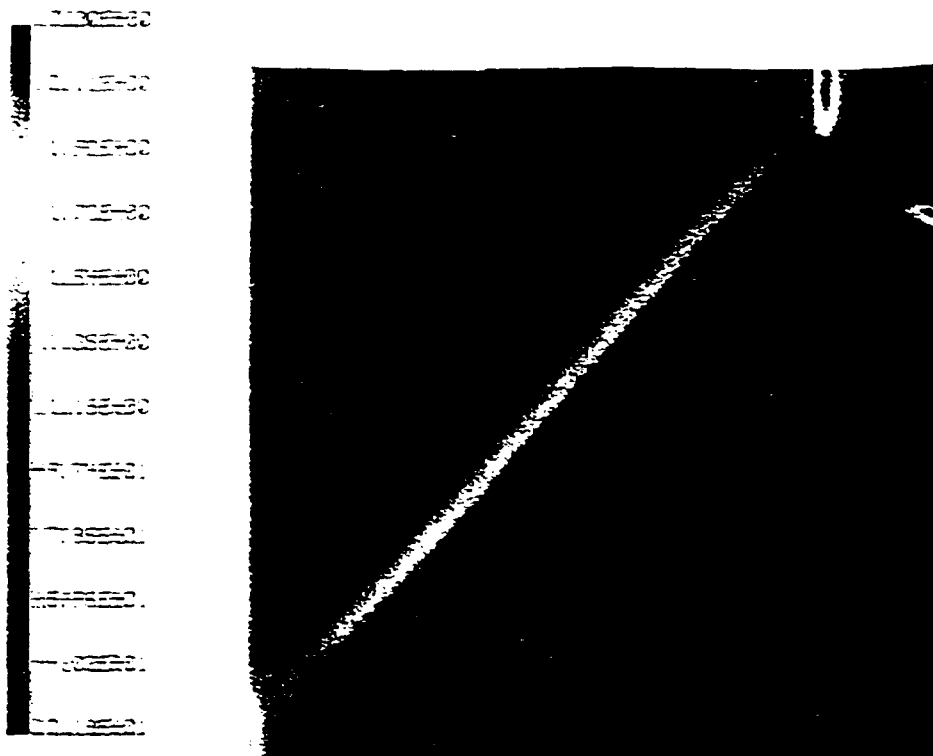


Fig. 1.8. Effective viscoplastic strain in the problem of Fig. 4 through 6 at $t = 7.25\mu\text{sec}$; 128×128 quadrilateral mesh, $r_0 = 0.1\text{mm}$.

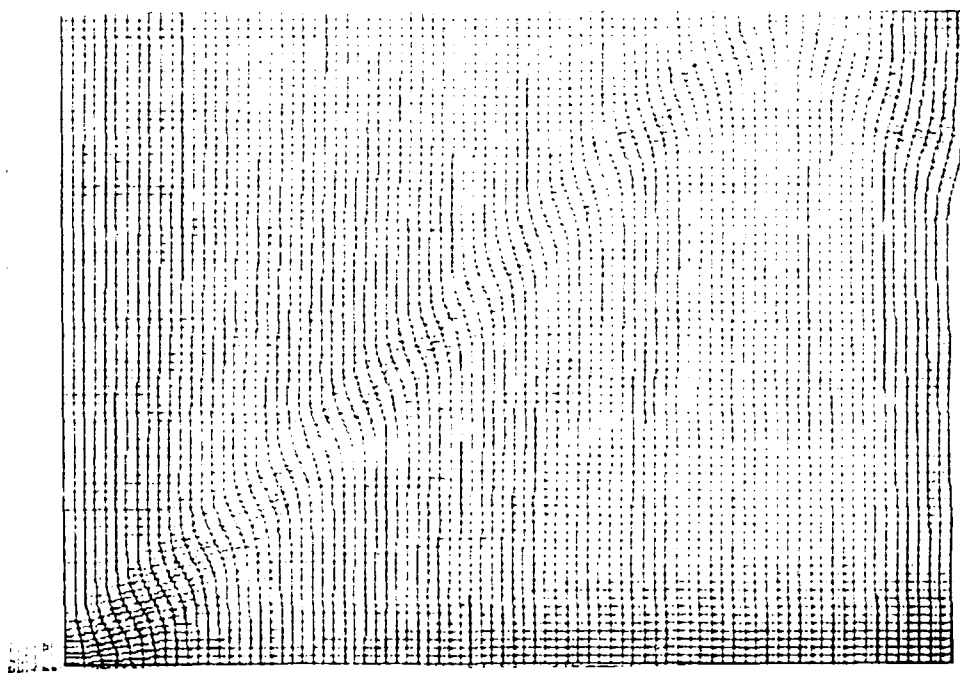


Fig. 1.9. Deformed mesh for 80×80 quadrilateral elements with $\alpha=0.2$ at $t = 4.79\mu\text{sec}$.

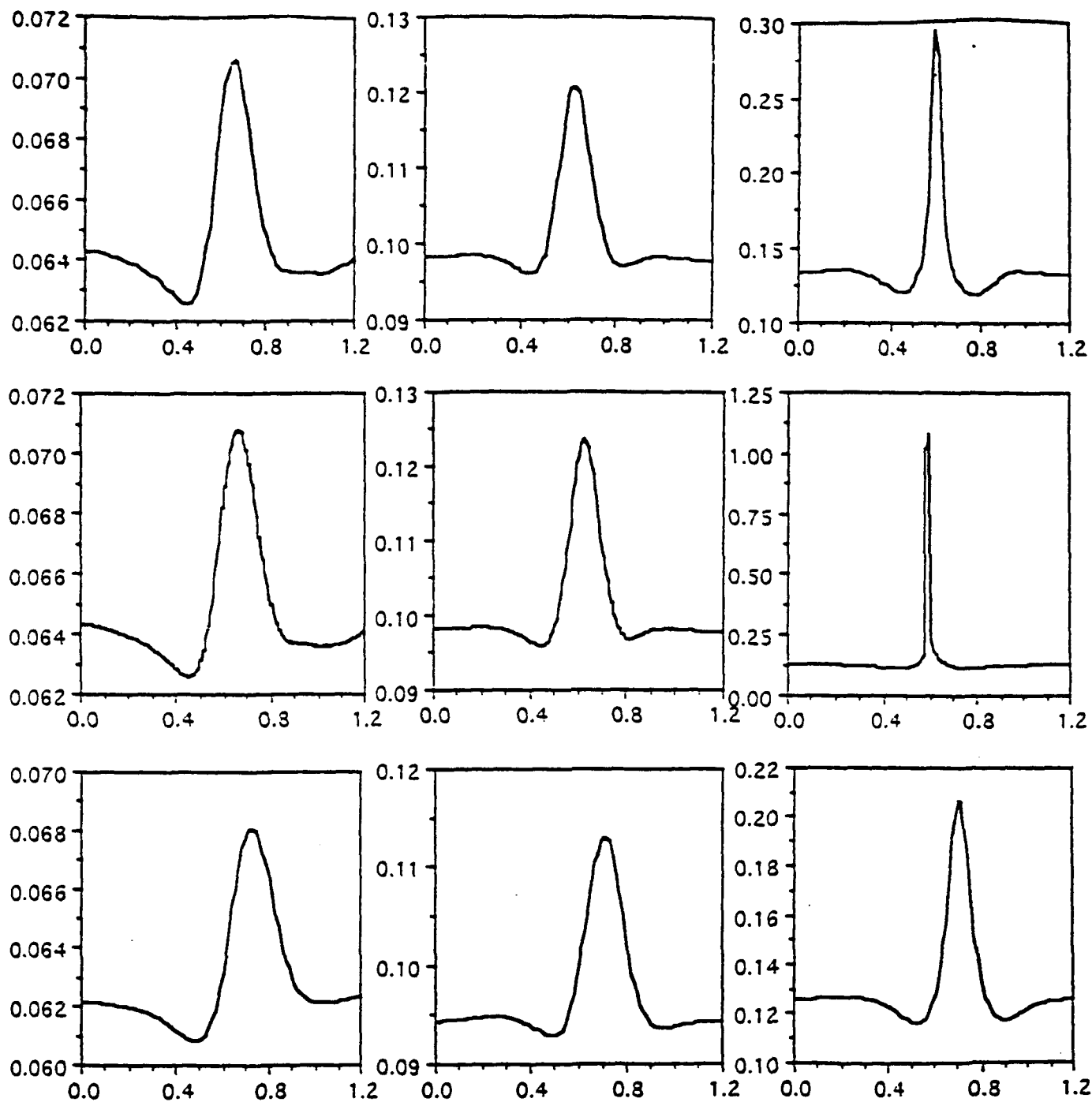


Fig. 1.10. Effective viscoplastic strain profiles across the shear band for quadrilaterals(top), the 128x128 crossed-diagonal triangular element mesh (middle) and quadrilaterals with selective-reduced integration SRI (bottom) at $t=2.0, 3.0, 4.0 \mu\text{sec}$, respectively, $r_0 = 0.1\text{mm}$; all meshes are 128x128.

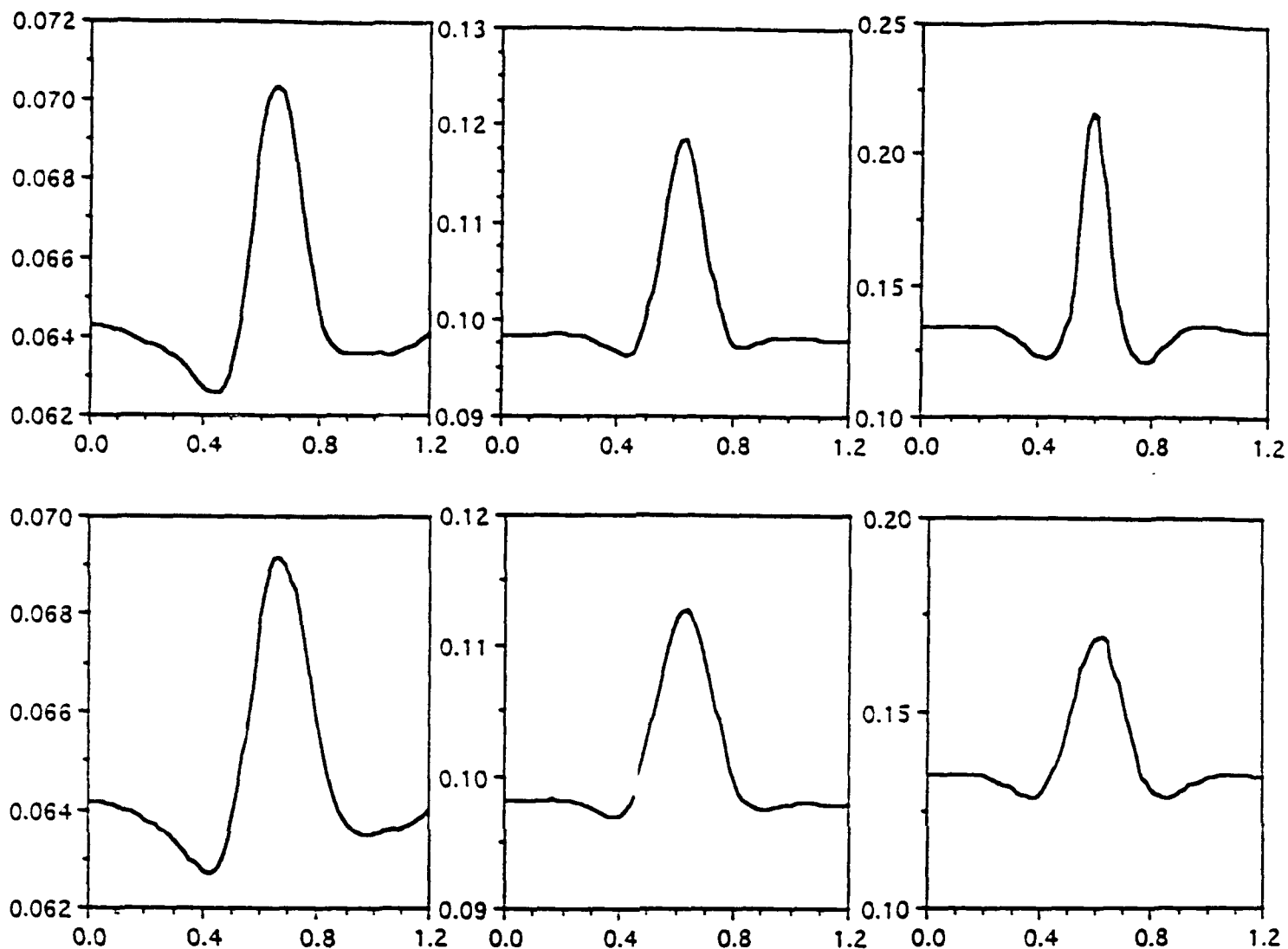


Fig. 1.11. Effective viscoplastic strain profiles across the shear band for quadrilateral 80x80 with stabilization parameters of 0.01 (top) and 0.05 (middle).

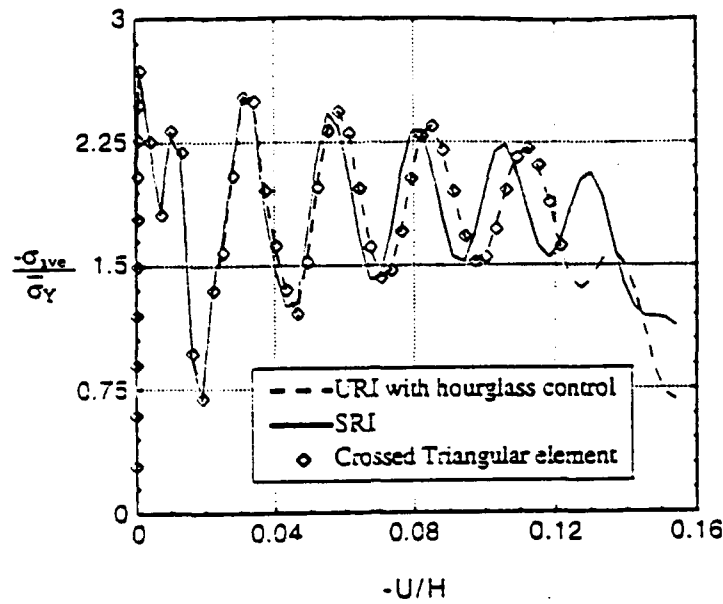


Fig. 1.12. Average stress versus end displacement curves for three types of elements in a 128x128 mesh: constant strain triangles, quadrilaterals with selective reduced integration (SRI) and quadrilaterals with one-point underintegration and stabilization (URI).

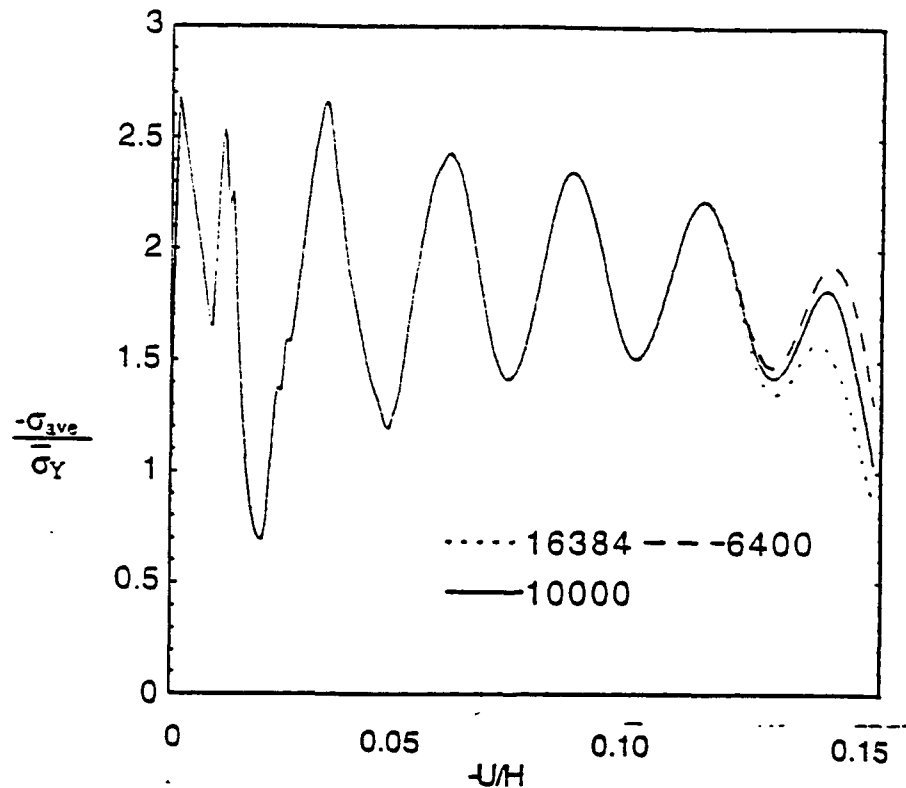


Fig. 1.13. Average stress versus end displacement curves for three meshes of one-point quadrature elements; 6,400 elements, 10,000 elements and 16,384 elements.

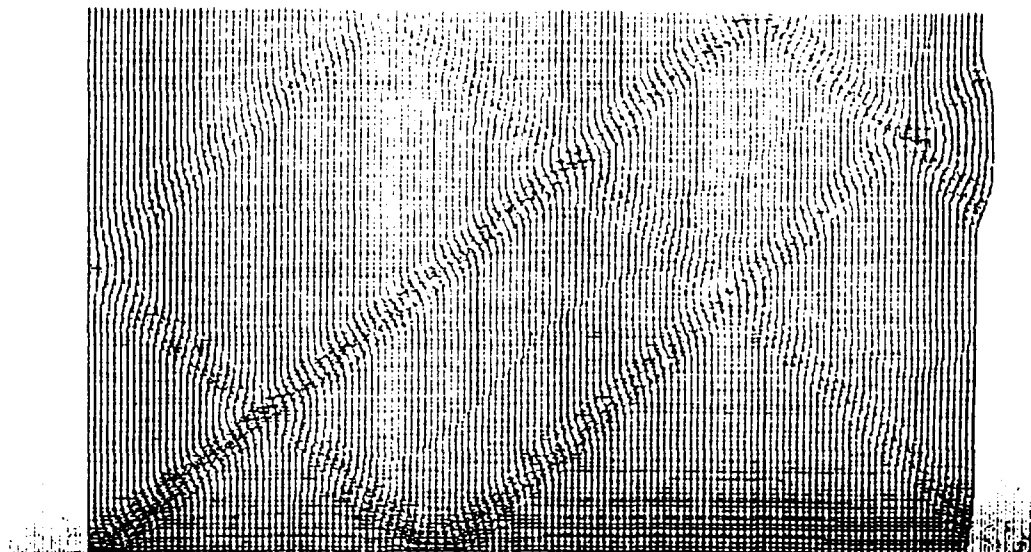


Fig. 1.14. Deformed mesh for small imperfection, $r_0=0.0039\text{mm}$, at $t=7.25\ \mu\text{sec}$, showing of multiple shear bands.

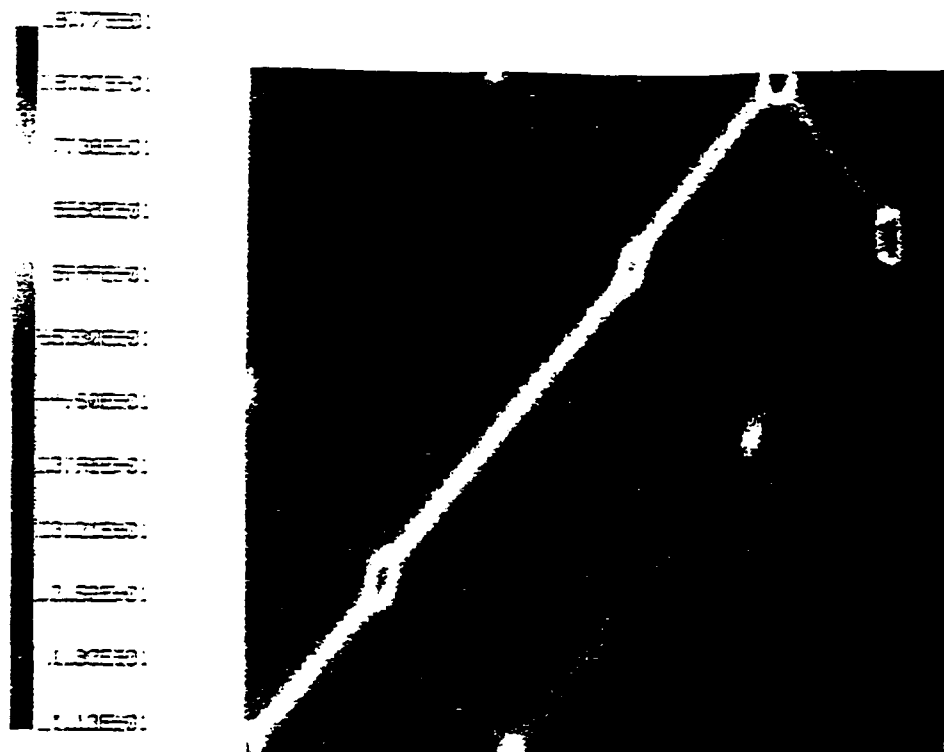


Fig. 1.15. Effective viscoplastic strain for small imperfection at $t=7.25\ \mu\text{sec}$; $r_0=0.0039\text{mm}$.

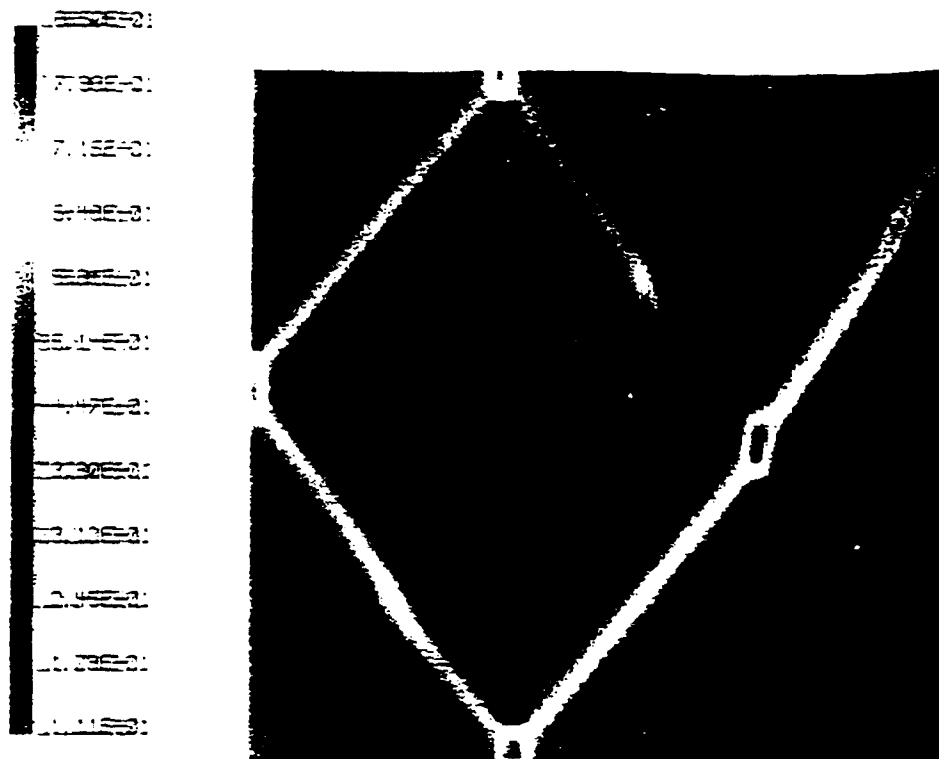


Fig. 1.16. Effective viscoplastic strain across the shear band for small imperfection at $t=7.25 \mu\text{sec}$ ($r_0=0.00195\text{mm}$) showing the development of multiple shear bands with markedly different strain distributions than in Fig. 15.

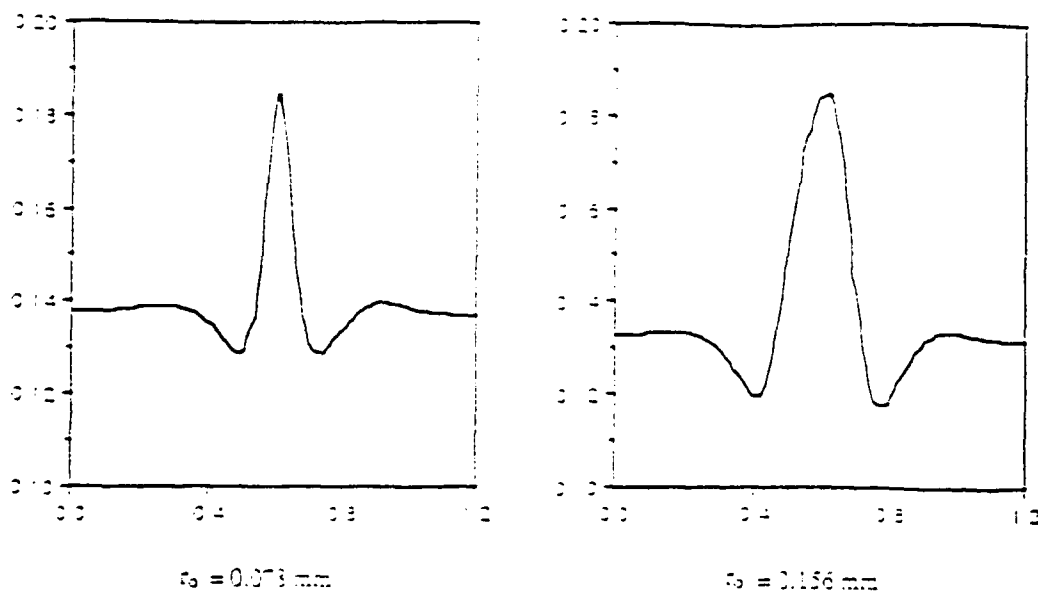


Fig. 1.17. Effective viscoplastic strain profiles across the band for the imperfection Eq.(18) at $t=4.0\mu\text{sec}$.

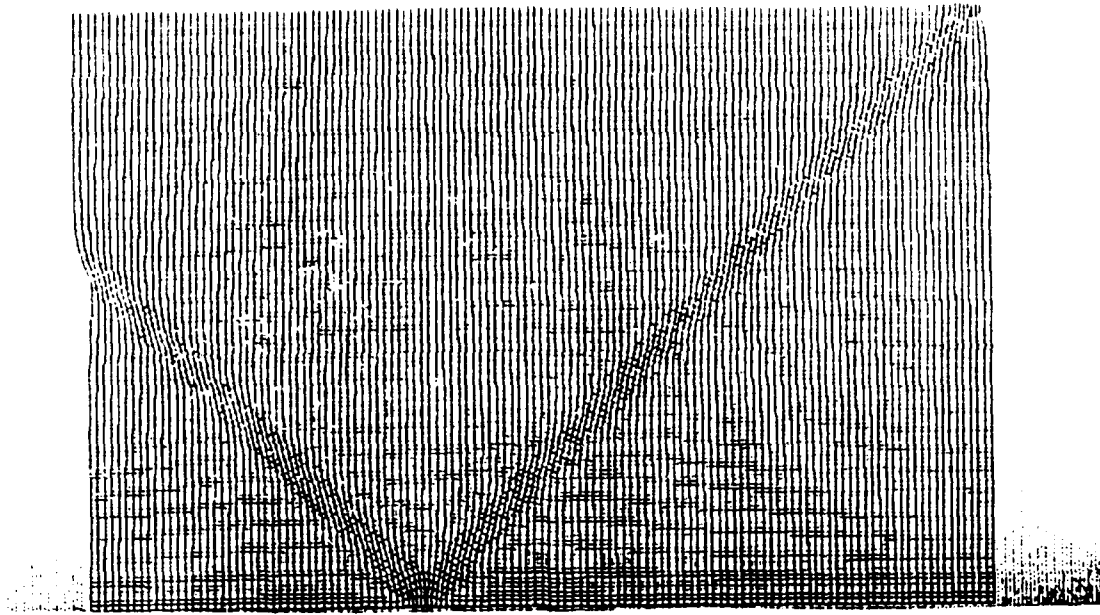


Fig. 1.18. Deformed mesh for upper *half* of specimen at $t=5.0\mu\text{sec}$ for imperfection at $x=-0.25\text{mm}$, $y=0.0$; $r_0=0.1\text{mm}$.

CHAPTER 2

H-ADAPTIVE FINITE ELEMENT METHODS FOR DYNAMIC PROBLEMS, WITH EMPHASIS ON LOCALIZATION

2.1. INTRODUCTION

The aim of this work is to develop methods for h-adaptive solutions of nonlinear transient problems with localization behavior. Localization occurs in rate independent materials when the momentum equations lose hyperbolicity; a regularization procedure based on damping known as a viscoplastic model will be used here which prevents loss of hyperbolicity. Even with regularization, the effect of a negative value of modulus is that severe deformations occur over narrow regions in which the strains and displacement gradients are very large; material response with negative tangent modulus are called strain-softening in engineering. Physically localization results in bands of high strain which are known as shear bands in the deformation of continua and as hingelines in the deformations of shells.

In developing these methods we have focused our efforts on explicit time integration methodologies and finite elements. Our focus on explicit time integration and finite elements is motivated by the fact that large scale engineering problems are almost exclusively solved by such methods; DYNA3D by Hallquist and Benson (1986) and its descendants today are the dominant tools for nonlinear transient problems of solid mechanics problems.

There is already a rich literature in adaptive methods for transient problems, so only a few works will be noted. Adaptive methods for hyperbolic problems were developed by Berger and Oliger (1984). They solved one and two dimensional transient problems with finite difference methods and used an error criterion based on Richardson extrapolation. Adjerid and Flaherty (1986) applied h-adaptive finite difference methods to parabolic problems. Drew and Flaherty (1984) applied adaptive space-time elements to one-dimensional shear banding.

In the finite element literature of solid mechanics, the application of h-adaptive methods to transient problems has been sparse, and we know of no applications of h-

adaptive finite element methods to transient problems with unstable material behavior, i.e. strain softening.

There have however, been a number of interesting related works. Ortiz and Quigley (1991) have used an r-adaptive method with an error criterion based on interpolation, Diaz et al (1983), to solve some static localization problems. Zeng and Wiberg (1992) developed an h-adaptive method based on constant strain triangular elements using a modification of the Zienkiewicz-Zhu (1987) or ZZ error criterion for linear wave problems. It has been proven by Rank and Zienkiewicz (1987) that for linear static problems this error criterion is equivalent to the Babuska-Rheinboldt (1978) criterion of the residual type.

One of the aims of this paper is to study various error criteria for this class of problems. The following error criteria were selected: The Zienkiewicz-Zhu (1987) L_2 -projection on stress, the Babuska-Rheinboldt (1978) residual criterion, and the interpolation criterion Diaz et al (1983). Though the first two of these were proposed for linear, elliptic problems, they appear to be reasonably effective in linear hyperbolic, one-dimensional problems. However, in localization problems they do not fare as well. Our studies show that the ZZ criterion, when formulated in terms of stresses is quite ineffective for localization problems. In fact, the stress field in and adjacent to a localization band which is triggered by strain-softening is nearly constant, so that the ZZ criterion never initiates refinement in the area of localization. Residual type criteria are similarly ineffective in localization.

In this paper we also propose an error criterion based on a L_2 projection of the strains. It is shown that this technique effectively captures the region where refinement, or what we call fission of elements, is needed. Results are obtained for several localization problems and compared to results obtained with very fine meshes. These results show that the present procedure is capable of achieving solutions of comparable accuracy with far fewer degrees of freedom.

The L_2 projection is more easily applied in a general finite element setting than interpolation criteria; the latter requires a knowledge of adjacent elements. It also appears to us simpler to apply than the local evolution equation approaches pioneered by Rank and further developed by Oden and coworkers (1989). In the latter, it is necessary to solve the governing equations with a bubble mode added to the element and an estimate of

the tractions at the element interface. Although these methods have proven very successful in two dimensional meshes (and are probably equally effective in three dimensional meshes), their application to shell structures looks formidable. It is not clear to us, for example, how these methods would be applied to a T-section or a box beam modeled by shell elements, whereas the L_2 strain projection is readily applied as described in Belytschko and Yeh (1992). Although general structures are not addressed in this paper, the objective is to develop error criteria suitable for transient analysis of nonlinear solids and continua.

An outline of the paper is as follows. In Section 2, the governing equations are reviewed. In Section 3, the error criteria used in this study are presented along with the new error criterion based on an L_2 strain projection. The adaptive technique is covered in Section 4. Numerical results for one dimensional and two dimensional problems are presented in Section 5, followed by a discussion and conclusions in Section 6.

2.2. GOVERNING EQUATIONS

The problems were solved by a finite element method with a Lagrangian mesh. The rate-of-deformation tensor

$$\eta_{ij} = \frac{1}{2} \left(\frac{\partial v_i}{\partial x_j} + \frac{\partial v_j}{\partial x_i} \right) \quad \text{or} \quad \eta = D \mathbf{v} \quad (1)$$

is used as a measure of deformation; here v_i are the velocities, x_i the Eulerian (spatial) coordinates. The material is characterized as an elastic-viscoplastic von Mises solid, the constitutive equation is expressed in terms of the Jaumann rate of the Cauchy stress

$$\overset{\nabla}{\sigma} = C(\eta - \eta^p) \quad (2)$$

where C is the initial elastic constitutive matrix. η^p is the viscoplastic strain rate given by

$$\eta^p = \frac{3\dot{\epsilon}}{2\bar{s}} \sigma' \quad (3)$$

with the stress deviator $\sigma' = \sigma - \frac{1}{3} \sigma : I$, where I is the identity tensor. The radius of the flow potential is $\sigma = (\frac{3}{2} \sigma' : \sigma')^{1/2}$. Here, the rate of the effective plastic strain, $\dot{\epsilon}$ is specified by the power law relation

$$\dot{\epsilon} = \dot{\epsilon}_0 [\bar{\sigma}/g(\dot{\epsilon})]^{1/m} \quad (4)$$

where $g(\dot{\epsilon})$ is the hardness function, m is the strain-rate hardening exponent and $\dot{\epsilon}_0$ is a reference strain rate.

$$\text{The momentum equation are } \sigma_{ij,j} + b_i = \rho \dot{v}_i \quad (5a)$$

in rectilinear coordinates, it can be written as

$$D^T \sigma + b = \rho \dot{v} \quad (5b)$$

where b is the vector of body forces and ρ is the mass density.

The finite element equations are obtained by approximating the velocities in each element by:

$$v(x,t) = N(x) \dot{d}(t) \quad (6)$$

The resulting ordinary differential equations are:

momentum equation

$$M a(t) = f(t) \quad a = \frac{\partial^2 d}{\partial^2 t} = \ddot{d}(t) \quad (7)$$

$$f(t) = f_{ext}(t) - f_{int}(t) \quad (8)$$

$$f_{ext} = \sum_e L_e^T f_{ext}^e(t) \quad f_{int} = \sum_e L_e^T f_{int}^e(t) \quad (9)$$

$$f_{int}^e(t) = \int_{\Omega_e} B^T(x,t) \sigma(x,t) d\Omega \quad (10)$$

measure of deformation

$$\eta(\mathbf{x}, t) = \mathbf{B}(\mathbf{x}) \dot{\mathbf{d}}_e(t) \quad \mathbf{B} = \mathbf{D} \mathbf{N} \quad (11)$$

$$\mathbf{d}_e(t) = \mathbf{L}_e \mathbf{d}(t) \quad (12)$$

In the above:

t = time;

\mathbf{M} = mass matrix;

\mathbf{d} = nodal displacement matrix;

$\mathbf{f}(t)$, $\mathbf{f}_{\text{ext}}(t)$, $\mathbf{f}_{\text{int}}(t)$ = resultant, external and internal nodal forces;

$\mathbf{B}(\mathbf{x})$ = semidiscrete form of the symmetric part of the gradient operator;

η = rate-of-deformation (velocity strain) tensor;

\mathbf{L}_e = Boolean connectivity matrix of element e .

2.3. ERROR MEASURES

The error is thought to be due to spatial discretization only, no attempt is done to quantify time integration error. However, the time integration scheme used here is an explicit central difference method which restricts the time step to a small critical value. The error is calculated using numerical integration with three point quadrature for the one dimensional problem and 2x2 quadrature for the two dimensional problems. We consider four types of element error measures:

(1) Zienkiewicz-Zhu (ZZ)

$$e_i^{\text{ZZ}} = \left[\int_{\Omega_i} (\bar{\sigma} - \sigma^h)^T (\bar{\sigma} - \sigma^h) d\Omega / \Omega_i \right]^{\frac{1}{2}} \quad (13)$$

This error criterion was first proposed for linear elastic problems (in the original ZZ criterion, the elastic coefficient matrix is included to give an error in energy, but it is omitted here to simplify application to nonlinear problems). Here Ω_i is the volume of element i , σ^h are the finite element solution for the stresses, and $\bar{\sigma}$ is the L_2 projection of the finite element stress which is given by (see Oden and Brauchli (1971), Zienkiewicz and Zhu (1987)):

$$\bar{\sigma}(\mathbf{x}) = \mathbf{N} \mathbf{s} \quad (14)$$

where \mathbf{s} is the array of the nodal value of the projected stress $\bar{\sigma}$, which is a C^0 function whereas σ^h is a C^{-1} function in these elements.

$$\mathbf{s} = \bar{\mathbf{M}}^{-1} \int_{\Omega} \mathbf{N}^T \sigma^h d\Omega \quad (15)$$

$$\bar{\mathbf{M}} = \int_{\Omega} \mathbf{N}^T \mathbf{N} d\Omega \quad (16)$$

$\bar{\mathbf{M}}$ is similar to the mass matrix and a lumped, diagonal form of the mass matrix obtained by Lobatto quadrature was used.

(2) Babuska-Rheinboldt (BR)

This is an error criterion developed for linear elliptic (static) problems. In applying their concept to transient problems, we consider the residual in the equations of motion.

$$e_i^{br} = \left[\{c_1 \int_{\Omega_i} r^2 d\Omega + c_2 \int_{\Gamma_i} J^2 d\Gamma\} / \Omega_i \right]^{\frac{1}{2}} \quad (17)$$

where in one dimensional problems

$$c_1 = \frac{h_i^2}{24k} \quad c_2 = \frac{h_i}{24k} \quad k = \frac{1}{1-\nu}$$

$$r = \sigma_{,x} + b - \rho \dot{v}$$

$$\mathbf{J} = \langle \mathbf{r} \rangle$$

where h_i is the length of element i , n is Poisson's ratio and $\langle \rangle$ is the jump operator, i.e. \mathbf{J} is the inter-element traction jumps.

(3) Interpolation (IN)

This criterion was developed by Diaz et al (1983) for static problems. The form we use here for dynamic problems is identical and in one dimension is given by:

$$e_i^{\text{in}} = \left[\frac{1}{h_i} \int_{h_i} (h_i u_{,xx})^2 dx \right]^{\frac{1}{2}} \quad (18)$$

where $u_{,xx}$ is obtained by using a quadratic Lagrange interpolant for constant strain elements. In general, a Lagrange interpolant one order higher than that used for the finite element solution is used. In one dimension

$$u_{,xx} = \frac{2u_1}{(x_1-x_2)(x_1-x_3)} + \frac{2u_2}{(x_2-x_1)(x_2-x_3)} + \frac{2u_3}{(x_3-x_1)(x_3-x_2)} \quad (19)$$

x_1 , x_2 , and x_3 are the coordinates of midpoints of elements $i-1$, i , $i+1$ for an interior element i . For an element i with a boundary on the right-hand side, the midpoints of $i-2$, $i-1$, i are used. For an element i with a boundary on the left-hand side the midpoints of i , $i+1$, $i+2$ are used. The displacements at x_1 , x_2 , and x_3 are denoted u_1 , u_2 , u_3 .

(4) Strain-Projection (SP)

The criterion proposed here is

$$e_i^{\text{sp}} = \left[\frac{1}{\Omega_i} \int_{\Omega_i} (\mathbf{\bar{\epsilon}} - \mathbf{\epsilon}^h)^T (\mathbf{\bar{\epsilon}} - \mathbf{\epsilon}^h) d\Omega \right]^{\frac{1}{2}} \quad (20)$$

where $\mathbf{\bar{\epsilon}}$ is evaluated by an L_2 projection which is identical to the L_2 projection of $\mathbf{\bar{\epsilon}}$. This measure represents the R.M.S strain error in an element and is convenient to use because it is nondimensional. The strain projection cannot be used directly at material interfaces because strains are generally discontinuous at such interfaces. The L_2 projection must

then be computed separately in each material subdomain; this procedure has been described by Belytschko and Yeh (1992).

2.4. ADAPTIVE PROCEDURE

We use an h-adaptive technique, we shall refer to the refinement of an element as 'fission' and to the unrefinement of a group (family) of four elements (siblings) to their parent element as 'fusion', see Belytschko et al (1989). These processes are illustrated in Fig. 1a. When an element is fissioned next to an unfissioned element, slave nodes are created. The motion of a slave node A is governed by the constraint of compatibility, i.e.

$$\mathbf{V}_A = \mathbf{T} \begin{Bmatrix} \mathbf{V}_1 \\ \mathbf{V}_2 \end{Bmatrix} \quad (21)$$

where \mathbf{T} is a linear operator which enforces compatibility and \mathbf{V}_1 and \mathbf{V}_2 are the velocities of the master nodes. When node A is midway between nodes 1 and 2, $\mathbf{T} = [\frac{1}{2} \mathbf{I}, \frac{1}{2} \mathbf{I}]$. The equations of motion are not evaluated at slave node but instead the nodal forces at slave nodes are added to forces at the corresponding master nodes, i.e.

$$\begin{Bmatrix} \mathbf{f}_1 \\ \mathbf{f}_2 \end{Bmatrix} = \begin{Bmatrix} \mathbf{f}_1 \\ \mathbf{f}_2 \end{Bmatrix}^* + \mathbf{T}^T \mathbf{f}_A \quad (2.22)$$

where \mathbf{f}_A are the nodal forces at the slave node and \mathbf{f}^* are the nodal forces at nodes 1 and 2 prior to the consideration of \mathbf{f}_A . This is a standard technique for treating constraints in explicit methods.

The adaptive process is driven by element error measures. An element is a candidate for fission when the error is more than a specified fission-limit e^{fi} , and a contiguous group of elements originating from a single parent element is a candidate for fusion when the error in all its siblings is lower than a specified fusion-limit e^{fu} . A candidate is only fissioned if it complies with the 1-irregular rule (Devloo et al (1987)) and the h_{min} requirement, where h_{min} is a prescribed lower limit on the size of an element. A candidate is fused if it complies with the 1-irregular rule only.

An important ingredient of an h-adaptive program is the data structure. In designing a data structure, compromises must be made to conserve storage and avoid

excessive computation time. In order to simplify the data structure we will enforce the 1-irregular rule, i.e. neighboring elements can be at most one generation apart. The nodal and element data for the adaptive process is handled by three arrays:

- (1) NSBLNG(4,NF): the four siblings of a family (Fig. 1a);
- (2) NABOR(8,NE): the eight neighbors of an element (Fig. 1b);
- (3) MGEN(NE): the number of descendant generations for an element.

where NE and NF are the number of elements and families in the mesh. NF is initially set to zero and increases (decreases) by one for each fissioned element (fused family). NSBLNG is used in the fusion process in order to identify elements of a family. NABOR is used in both fission and fusion to determine the appropriate numbering, connectivity and status of nodes; it is also used to identify nodes lying on a boundary. MGEN is required in order to comply with the 1-irregular rule.

In order to clarify the use of the above arrays, let us consider mesh 'a' shown in Fig. 1c with element 5 already fissioned. Also consider mesh 'b' obtained by fissioning element 2. The NABOR array for element 2 is given in Table 1 for both meshes. The first thing to notice is the zero entries for L7 and L8, indicating a boundary to the left-hand side of element 2; thus a new node needs to be created (node 20), which is a master node. Next, L1=L2=1 indicating that element 1 extends along the entire side of element 2 and thus a new node (node 18) needs to be created, which is a slave node. Now, L3=5 and L4=9 thus a node already exists (node 16) which was a slave node in mesh 'a' and will become a master node upon fission of element 2. The NSBLNG array (Table 2) gives the four siblings for the only family in mesh 'a', so elements 5,7,8 and 9 are the only members of the mesh whose error is checked against e^{fu} .

We will implement the repeat algorithm employed by Belytschko and Yeh (1992). The basic idea is as follows. Start at time $t=0$ with an initial coarse mesh 'a' (Fig. 2) and solve the problem using a time increment Δt for an elapsed time t_1 , during which the mesh is modified at times $a=1/n$, $n \geq 1$; and ends up as mesh 'b'. Now, we go back to $t=0$ and use mesh 'b' to solve the problem and record the results. So the first run over the time interval serves the purpose of finding a suitable mesh while the second run is used to actually solve the problem at hand. This procedure is repeated over every time interval t_1 as illustrated in Fig. 2 thus using mesh 'c' to go from $t=t_1$ to $t=2t_1$; and so on until the end time t_2 is reached.

Although the above description was limited to a four-node quadrilateral, it is also applied to the two node element for the one dimensional problems solved here. Fig. 1a shows the fission-fusion process for one element, in this case there is no need for slave nodes, i.e. all nodes are masters. Fig. 1b shows L1 and L2 the two neighbors of element JE. The same three arrays: NSBLNG, NABOR, MGEN are used, however the size of NSBLNG reduces to $2 \times N_F$ and that of NABOR to $2 \times N_E$.

2.5. NUMERICAL EXAMPLES

Stability considerations

The explicit integration schemes for the semi-discrete equations of motion (Eqn. 7) and the plastic strain rate (Eqn. 4) are conditionally stable. In addition since h-adaptivity introduces much smaller elements, subcycling in which different time steps are used in different elements was used to achieve computational efficiency, see Belytschko and Liu (1982) and Belytschko and Lu (1992).

One dimensional bar

Consider a bar of length $L=100$ in, cross-sectional area $A=1.0$ in², elastic modulus $E=3 \times 10^7$ lbf/in², density $\rho=0.00074$ lb/in³. The element mass matrix is $M = \frac{1}{2} (M^{\text{diag}} + M^{\text{cons}})$ where M^{diag} is the diagonal, lumped mass and M^{cons} is the consistent mass. It is well known that this combination provides the best spectral fidelity for the mesh.

The material is rate-dependent with an effective plastic strain rate represented by the power law relation given by Eqn. 4. The evolution equation (Needleman 1988) for $g(\dot{\epsilon})$ takes the form $\dot{g} = H |\dot{\epsilon}|$, where $H = H_1$ for $\dot{\epsilon} \leq \dot{\epsilon}_m$, $H = H_2$ for $\dot{\epsilon} > \dot{\epsilon}_m$ and $g(0) = \sigma_0$. At each time increment the stress state is updated using the forward Euler scheme. Fig. 3 shows computed stress-strain curves (A, B, and C) at various imposed strain rates for $\sigma_0 = 0.002E$, $m=0.02$, $\dot{\epsilon}_0=0.002$, $H_1=25\sigma_0$, $H_2=2.5\sigma_0$ and $\dot{\epsilon}_m=0.2\sigma_0/E$. As apparent from these curves the material hardens with increasing strain, but because of strain-rate dependence softening might still occur.

The bar is subjected to a constant velocity $v_0=300$ in/s at both ends resulting in two step waves of constant strain traveling toward each other. The magnitude of the

velocity is chosen so that the material remains elastic until the waves meet at the middle of the bar, doubling the strain value at that point and driving the material well into the plastic range. At first thought, no localization is expected since the material is hardening under constant strain rates, but a closer look at the actual stress-strain response (Curve D, Fig. 3) for the midpoint under this particular loading shows a softening behavior which is due to the step strain wave. Solving this example using a fixed mesh with 80 elements, $\Delta t = 2.5 \times 10^{-7}$, and $t_2/\Delta t = 1800$ results in a localized strain profile B in Fig. 4a and a stress profile as shown in Fig. 4b. We will use these results as a benchmark for the adaptive results. These profiles are plotted for $t = 0.9t_0$, where t_0 is the time required for an elastic wave to traverse the entire length of the bar, $t_0 = L/\sqrt{E/\rho}$.

It is important, however, to keep in mind that in problems involving localization due to material softening, the late stages of the solution depend on the element size employed in the analysis. A simple remedy for this is to restrict the minimum size of elements used to a minimum allowable size; we used $h_{\min} = L/80$ for all runs. This is appropriate here, since our goal is to illustrate adaptivity and not to propose a constitutive law that overcomes this dependence on mesh size which occurs in the late stages of localization even with viscoplasticity.

In the results for the fixed mesh all four estimates indicate high error at the wave fronts before the two waves meet ($t < 0.5t_0$). However, after the waves meet, Fig. 5, only the SP and IN indicate high errors at wave fronts and localization regions, while the ZZ and BR indicate high errors at wave fronts only, thus missing the localization. Although the above error profiles are shown for $t = 0.9t_0$, they are representative of profiles for $t > 0.5t_0$. The SP and IN estimates are normalized with respect to $\epsilon_0 = \sigma_0/E$, while the ZZ and BR are normalized with respect to s_0 . The normalized SP estimates the error at wave fronts to be around 0.05 (Fig. 5a) which is the same as the estimate given by the normalized ZZ (Fig. 5c), this is expected because in this region the behavior is elastic and the two estimates are identical. The normalized ZZ and BR profiles (Fig. 5c,d) are very close, which is expected in linear static problems and seems to carry over to dynamics in this specific example.

This one dimensional example was also solved using an adaptive mesh guided by ZZ ($e^{\text{fi}} = 0.02\sigma_0$ and $e^{\text{fu}} = 0.5e^{\text{fi}}$) and SP ($e^{\text{fi}} = 0.02\epsilon_0$ and $e^{\text{fu}} = 0.5e^{\text{fi}}$) with $\Delta t = 2.5 \times 10^{-7}$, $t_1/\Delta t = 100$, $t_2/\Delta t = 1800$, $\alpha = 0.2$, and $h_{\min} = L/80$. The evolution of the adaptive meshes with time are shown in Fig. 6. The meshes are similar until localization occurs ($t = 0.5t_0$),

the ZZ driven mesh (Fig. 6a) does not refine the mesh to accommodate the localization while the SP does (Fig. 6b). Thus the strain profiles after localization are not the same, with the SP driven one being closer to the fixed mesh (Fig. 4a). Results obtained by using IN are similar to that of SP, while results obtained by using BR are similar to that of ZZ.

Compression of a rectangular block

Consider the problem of plane strain compression analyzed by Needleman (1989) for dynamic shear band development. The main difference between Needleman's analysis and ours lies in the type of discretization; we use four-node quadrilaterals with one point integration and hour-glass control (Flanagan and Belytschko (1981)), Needleman used crossed triangular quadrilaterals. We use one point integration and perturbation hourglass control (with a viscosity factor of 0.01) in order to be able to represent incompressible deformation without mesh locking and for speed of calculation.

The uniaxial response for the effective plastic strain rate is represented by a power law rate relation (Eqn. 4) with a hardness function

$$g(\epsilon) = \sigma_0 \frac{(1 + \epsilon/\epsilon_0)^N}{1 + (\epsilon/\epsilon_1)^2} \quad (23)$$

An initial imperfection is included in the form of a reduction in the yield strength

$$\sigma_0 = \bar{\sigma}_0 (1 - \gamma e^{-r^2/r_0^2}) \quad r^2 = x^2 + y^2 \quad (24)$$

The material properties used are as follows: Young's Modulus $E=211\text{GPa}$, Poisson's ratio $\nu=0.3$, mass density $\rho = 7800 \text{ kg/m}^3$, $\gamma=0.2$, $r_0 = 0.1\text{mm}$, $\bar{\sigma}_0=460\text{MPa}$, $\epsilon_0=0.00218$, $N=0.1$, $m=0.01$ and $\dot{\epsilon}_0=0.002 \text{ s}^{-1}$.

We analyze one fourth of the block ($h_0 \times h_0$) shown in Fig. 7 by making use of symmetry. The prescribed velocity $v(t)$ is equal to $v_0 t/t_0$ for $t \leq t_0$ and v_0 for $t > t_0$ with $t_0=0.1 \times 10^{-6}$. The end displacement and the corresponding average stress are given by:

$$u = \int_0^t v(t) dt \quad \text{and} \quad \sigma_{\text{avg}} = \frac{1}{h} \int_0^{h_0} t_y(x, h_0) dx \quad (25)$$

where t_y is the traction in the y-direction and h is the current width at $y=h_0$. At each time increment, the stress state is updated using the rate tangent method of Peirce et al. (1984) with the integration parameter $q=1.0$.

Case 1

As a first step, we used a fixed mesh of 20×20 elements with two forms of the hardness function $g(\epsilon)$: (a) hardening with $\epsilon_1 = 10^4 \epsilon_0$ and (b) softening with $\epsilon_1 = 10^2 \epsilon_0$. Fig. 8 shows average stress versus end displacement, with an imposed velocity $v_0 = 10$ m/s, $\Delta t = 2.0 \times 10^{-9}$, $t_2/\Delta t = 6000$ for the two materials (Curves A,C). The response for both materials is initially identical; however, for the softening material there is an abrupt stress drop with increased loading that is associated with shear band formation. For the softening solid a region of high effective strain, ϵ , starts developing at $-u/h_0 = 0.06$ and acquires the shape shown in Fig. 9a for the last calculated point, $-u/h_0 = 0.12$. A definite band with high strains forms at 45° to the compression axis. The strains inside the band increase significantly with continued loading, while regions outside this band experience little change in strain. This is not the case for the hardening solid, where strains increase uniformly throughout the solid with increased loading (Fig. 9b). However, only a small region of higher strains develops near the inhomogeneity.

Fig. 10 shows the surfaces of the SP error corresponding to the surfaces of effective strains shown in Fig. 9. For the softening solid, the error is high in the entire shear band region (Fig. 10a). For the hardening solid, the SP error is large only at the inhomogeneity location (Fig. 10b). These results are desirable and will lead to a useful mesh: refinement occurs near the inhomogeneity for hardening, and within the whole shear band for softening.

Starting with an initial mesh of 20×20 elements, and using the SP error measure to guide adaptivity with $e^{fi} = 0.01$, $e^{fu} = 0$, $Dt = 1.0 \times 10^{-9}$, $t_1/\Delta t = 800$, $t_2/\Delta t = 8000$, and $\alpha = 0.5$ the softening solid was solved. The response curve D is shown in Fig. 8. Labels 1 to 6 are used to show the evolution of the mesh with increased loading. Each segment of the curve between labels represents a different mesh. For the first segment (0-1) no refinement is needed, for segment 1-2 only few element at the lower left corner of the mesh are fissioned. For segment 2-3 the refinement is minimal and is limited to a region near the imperfection (Fig. 11a). However, for segments 3-4, 4-5, and 5-6 which involve

localization, the entire shear band region is refined to give the meshes in Fig. 11b, c, d respectively. In this analysis we use $h_{\min}=h_0/80$, which allows for only two levels of fission.

Curves B, C and D (Fig. 8) are for the same problem, the only difference being in the size of the smallest elements in the shear band. Although the curves are identical up to about $-u/h_0=0.05$, the response becomes noticeably different as the loading progresses. In order to compare the responses obtained for $-u/h_0>0.05$ we consider: (1) the onset of localization to be defined as the point on the curve after which the first abrupt drop in stress occurs, and (2) the magnitude of this drop to be a gauge for the severity of the localization. Curve D predicts an earlier onset of localization with high severity followed by high oscillations, while Curve B predicts a late onset with low severity followed by low oscillations. Curve C is middle grounds between B and D.

Case 2

The imperfection of case 1 is eliminated, i.e. $\gamma=0$ in Eqn. 24. Using a fixed mesh of 20×20 elements with $v_0=10$ m/s, $\Delta t=2.0 \times 10^{-9}$, $t_2/\Delta t=6000$, and solving the case of a softening solid ($\epsilon_1=10^2 \epsilon_0$), we obtain curve A in Fig. 12. Although there is no imperfection in this case, a region of high effective strain starts developing at $-u/h_0=0.10$ and acquires the shape shown in Fig. 13a for the last calculated point, $-u/h_0=0.12$. The mode of localization is quite different than that of case 1 (Fig. 9a) and occurs at a later stage of loading: $-u/h_0=0.10$ as compared to 0.06 for case 1. Thus, in this problem, an imperfection is not needed to achieve localization and the pattern of shear bands is quite different than with an imperfection. The plot for the SP error at $-u/h_0=0.12$ (Fig. 13b) indicates high error in the localized region. This will lead to refinement within the whole shear band.

The problem was also solved starting with an initial mesh of 20×20 elements, and using the SP error measure to guide the adaptivity with $e^{fi}=0.02$, $e^{fu}=0$, $\Delta t=1.0 \times 10^{-9}$, $t_1/\Delta t=12000$, $t_2=t_1$, $\alpha=1/15$, and $h_{\min}=h_0/80$. The response curve B is shown in Fig. 12 and the corresponding adaptive mesh is shown in Fig. 14.

Curves A and B in Fig. 12 are the response curves for the same problem, the only difference being in the size of the smallest elements in the shear band. The curves are identical up to the onset of localization after which Curve B shows a steeper stress drop followed by higher oscillations; this result is similar to case 1.

Case 3

In this case we consider a softening solid with $\epsilon_1=200\epsilon_0$ and impose a velocity $v_0=30$ m/s. This case is identical to the one analyzed by Belytschko et al (1992) using a fine mesh with 128×128 elements. We start with an initial coarse mesh (16×16 elements) and use the SP error measure to guide the adaptivity. Fig. 15b shows the curve of the average stress versus end displacement corresponding to the adaptive mesh shown in Fig. 15a. This curve is in good agreement with the one for the fine mesh (128×128) represented by discrete points in Fig. 15b. The adaptive mesh suggests the existence of a shear band. This can be verified by plotting the profile of the effective strains across the band along the normal direction at $-u/h_0=0.12$ (Fig. 15c). This profile is also in good agreement with the results for the fine mesh.

2.6. CONCLUSIONS

The following error estimates have been studied in one-dimensional localization problems: the Zienkiewicz-Zhu global L_2 stress, Babushka-Rheinboldt residual criterion, the interpolation criterion of Diaz et al (1983), and the strain-projection. The last is a new error criterion proposed herein which is based on an L_2 projection of strains.

It was shown that error indicators such as the momentum equation residual (developed by Babushka & Rheinboldt (1978) for linear elastic statics) and the L_2 projection on stresses (developed by Zienkiewicz & Zhu (1987) for linear elastic statics) are not effective for localization problems. They fail to indicate the need for refinement in the area of localization, where the strain gradients are very large but the stress is nearly uniform.

An interesting finding from the adaptive two dimensional calculations is that in the dynamic problem, imperfections interact with the amplification due to wave propagation effects to set the shear band pattern. In static problems with homogeneous stress fields, the imperfection is critical in setting the localization and the length scale (i.e. the internal structure) of the shear band. Thus if a large imperfection is placed at the center, a pattern of shear bands, with one passing through the middle develops. Otherwise, a different pattern of shear bands develops.

It is also of interest to note that while nonuniform meshes in wave propagation problems lead to additional errors due to spurious reflection at interfaces between regions

with different element sizes (Holmes and Belytschko (1976)), in adaptive methods, varying element sizes do not detract from accuracy. The reason for this is evidently the tendency of the fine mesh to move with the wave front, so that the wave front does not pass through regions of different element sizes. In fact, the coarser elements away from the wave front are beneficial because they filter out spurious high frequency components.

The results obtained here make us quite optimistic about the potential of h-adaptivity in explicit, transient finite element programs. The implementation of h-adaptivity in this class of programs is not difficult, since slave nodes which arise at mesh gradations are easily handled in an explicit setting. Furthermore, the overhead associated with adaptivity is not large, and a more accurate solution can be obtained with the same computational resources. The regions of localization cannot be known prior to a run, and the use of a uniform mesh with the refinement necessary to resolve shear bands accurately requires excessive computational resources. For general purpose programs, the addition of h-adaptivity is more difficult, but nevertheless the advantages are promising.

REFERENCES

- Adjerid S. and Flaherty J.E. (1986), "A moving-mesh finite element with method with local refinement for parabolic partial differential equations." *Computer Methods in Applied Mechanics and Engineering*, **55**, 3-26.
- Babushka I. and Rheinboldt (1978), "Error estimates for adaptive finite element computations." *SIAM Journal of Numerical Analysis*, **15**, 736-754.
- Belytschko T., Chiang H.Y., and Plaskacz E. (1992), "High resolution two dimensional shear band computations: imperfections and mesh dependence." *Computer Methods in Applied Mechanics and Engineering* (to appear).
- Belytschko, T. and Liu W.K. (1982), "Time integration with explicit/explicit partitions EPIC-2." Report to Ballistics Research Laboratory.
- Belytschko, T. and Lu Y.Y. (1992), "Convergence and stability analyses of multi-time step algorithm for parabolic systems." *Computer Methods in Applied Mechanics and Engineering* (to appear).
- Belytschko T., Wong B.L., and Plaskacz, E.J. (1989), "Fission-Fusion adaptivity in finite elements for nonlinear dynamics of shells." *Computers and Structures*, **33**, 1307-1323.
- Belytschko T. and Yeh I.S. (1992), "The splitting pinball method for contact-impact problems." *Computer Methods in Applied Mechanics and Engineering* (to appear).
- Berger M. and Oliger J. (1984), "Adaptive mesh refinement for hyperbolic partial differential equations." *Journal of Computational Physics*, **53**, 484-512.
- Devloo P., Oden J.T., and Stroubelis (1987), "Implementation of an adaptive refinement technique for the SUPG algorithm." *Computer Methods in Applied Mechanics and Engineering*, **61**, 339-358.
- Diaz A.R., Kikuchi P., and Taylor J.E. (1983), "Design of an optimal grid for finite element methods." *Journal of Structural Mechanics*, **11**(2).

Drew D.A. and Flaherty J.E (1984), "Adaptive finite element methods and the numerical solution of shear band problems."

Flanagan D. and Belytschko T. (1981), "A uniform strain hexahedron and quadrilateral with orthogonal hourglass control." *International Journal for Numerical Methods in Engineering*, **17**, 679-706.

Hallquist J.O. and Benson D.J. (1986), "Nonlinear dynamics analysis of structures in three dimensions." *DYNA3D user's manual*, Report UCID-19592, University of California, Lawrence Livermore National Laboratory, Livermore, CA.

Holmes N. and Belytschko T. (1976), "Postprocessing of finite element transient response calculations by digital filters." *Computer & Structures*, **6**, 211-216.

Needleman A. (1988), "Material rate dependence and mesh sensitivity in localization problems." *Computer Methods in Applied Mechanics and Engineering*, **67**, 69-85.

Needleman A. (1989), "Dynamic shear band development in plane strain." *Journal of Applied Mechanics*, **56**, 1-9.

Oden J.T. and Brauchli (1971), "On the calculation of consistent stress distributions in finite element applications." *International Journal for Numerical Methods in Engineering*, **3**, 317-325.

Oden, J.T., Demkowicz, L., Rachowicz, W., and Westermann, T.A. (1989), "Toward a universal h-p adaptive finite element strategy, part 2. A posteriori error estimation." *Computer Methods in Applied Mechanics and Engineering*, **77**, 113-180.

Ortiz, M. and Quigley, J. (1991), "Adaptive mesh refinement in strain localization problems." *Computer Methods in Applied Mechanics and Engineering*, **90**, 781-804.

Peirce D., Shih C.F., and Needleman A. (1984), "A tangent modulus method for rate dependent solids." *Computers and Structures*, **18**, 875-887.

Rank E. and Zienkiewicz (1987), "A simple error estimator in the finite element method." Communications in applied numerical methods, **3**, 243-249.

Zeng L.F. and Wiberg N.-E. (1992), "Error estimation and adaptivity of spatial discretization in semidiscrete finite element analysis for dynamic problems." Computational Mechanics.

Zienkiewicz, O.C. and Zhu, J.Z. (1987), "A simple error estimator and adaptive procedure for practical engineering analysis." International Journal for Numerical Methods in Engineering, **24**, 337-357.

	JE	NABOR								MGEN
		L1	L2	L3	L4	L5	L6	L7	L8	
Mesh a	2	1	1	5	9	3	3	0	0	0
Mesh b	2	1	1	10	10	12	12	0	0	1

Table 1

NSBLNG	Mesh a	Mesh b	
M1	5	5	2
M2	7	7	10
M3	8	8	11
M4	9	9	12

Table 2

Captions

Fig. 2.1. (a) Fission-fusion cycle for a four-node quadrilateral and a two-node bar, (b) neighbor configuration for a four-node quadrilateral and a two-node bar, (c) transition from mesh **a** to mesh **b** by fission of element 2.

Fig. 2.2. Repeat algorithm for an initial mesh with four elements.

Fig. 2.3. Stress-strain response at various constant strain rates (A,B,C) and a variable strain rate (D).

Fig. 2.4. Comparison of (a) strain and (b) stress profiles for a fixed 80 element mesh (80), with adaptive solutions using Zienkiewicz-Zhu error criterion (ZZ) and strain-projection error criterion (SP).

Fig. 2.5. Error profiles for one dimensional localization problem using: (a) strain projection (SP), (b) interpolation (IN), (c) Zienkiewicz-Zhu (ZZ), and (d) Babushka-Rheinboldt (BR).

Fig. 2.6. Evolution of mesh with time guided by (a) Zienkiewicz-Zhu and (b) strain projection error measures.

Fig. 2.7. Block subjected to compression.

Fig. 2.8. Average stress versus end displacement curves for the block using a hardening material (Curve A) and a softening material (Curves B, C,D).

Fig. 2.9. Effective strain surfaces at $-u/h_0=0.12$ corresponding to (a) Curve C and (b) Curve A in Fig. 2.8.

Fig. 2.10. Strain projection error surfaces at $-u/h_0=0.12$ corresponding to (a) Curve C and (b) Curve A in Fig. 2.8.

Fig. 2.11. Adaptive mesh evolution corresponding to Curve D in Fig. 2.8.

Fig. 2.12. Average stress versus end displacement curves for a softening material with no imperfection.

Fig. 2.13. (a) Effective strain and (b) Strain projection error surfaces corresponding to Curve A (Fig. 2.12) at $-u/h_0=0.12$.

Fig. 2.14. Adaptive mesh corresponding to Curve B (Fig. 2.12.).

Fig. 2.15 (a). adaptive mesh, (b). Average stress versus end displacement curve for a softening solid and (c). Effective strain across the shear band along the normal direction.

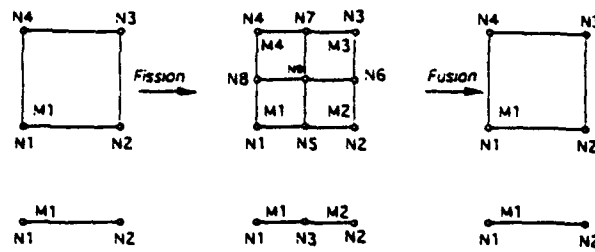
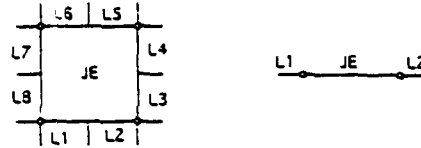
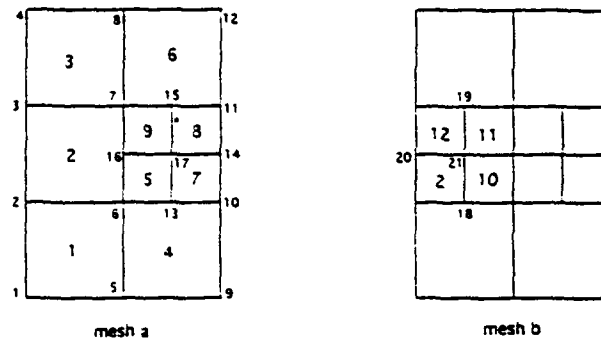


Fig. 2.1. (a) Fission-fusion cycle for a four-node quadrilateral and a two-node bar



(b) neighbor configuration for a four-node quadrilateral and a two-node bar



(c) transition from mesh a to mesh b by fission of element 2.

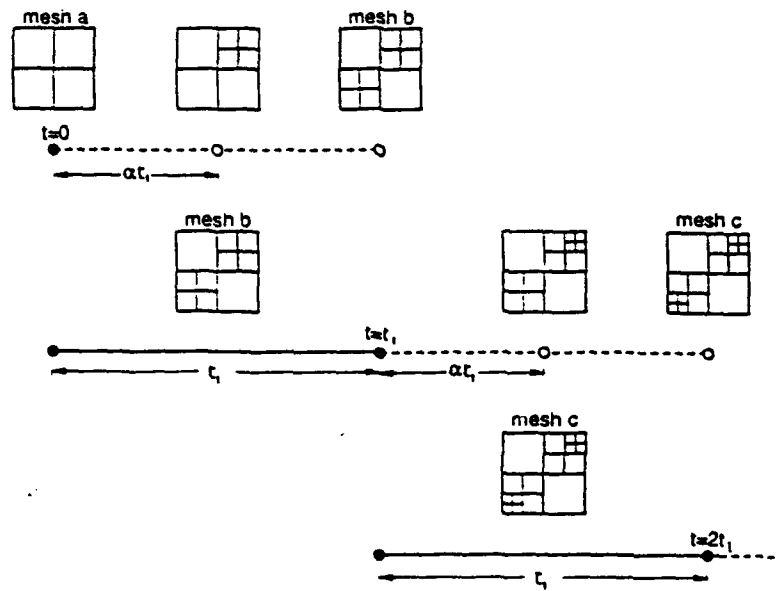


Fig. 2.2. Repeat algorithm for an initial mesh with four elements.

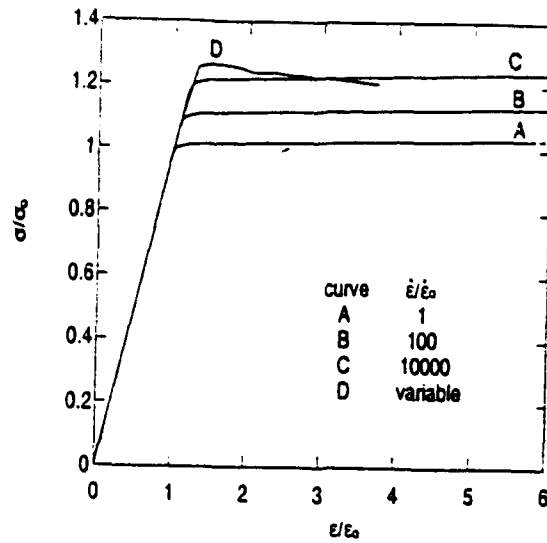


Fig. 2.3. Stress-strain response at various constant strain rates (A,B,C) and a variable strain rate (D).

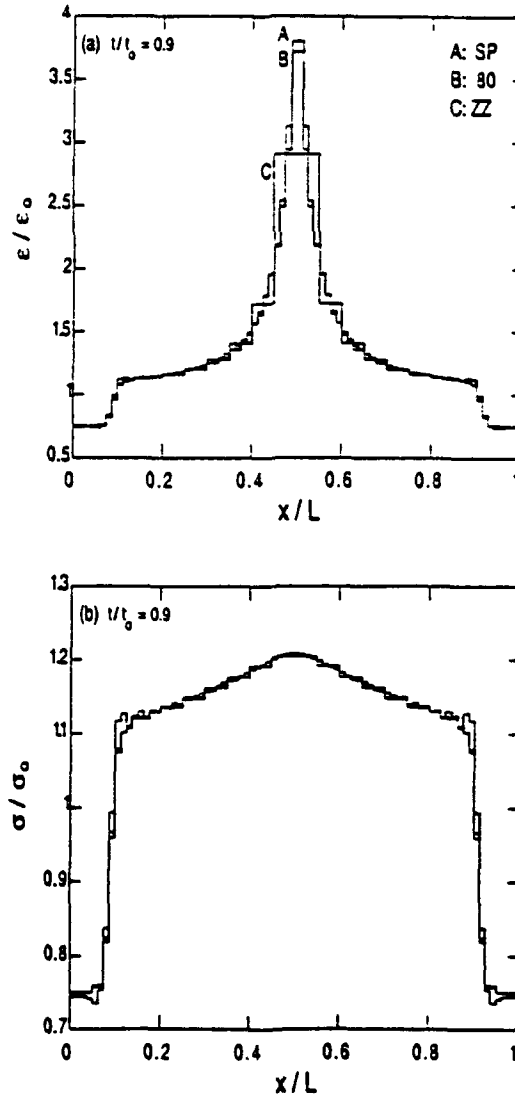


Fig. 2.4. Comparison of (a) strain and (b) stress profiles for a fixed 80 element mesh (80), with adaptive solutions using Zienkiewicz-Zhu error criterion (ZZ) and strain-projection error criterion (SP)

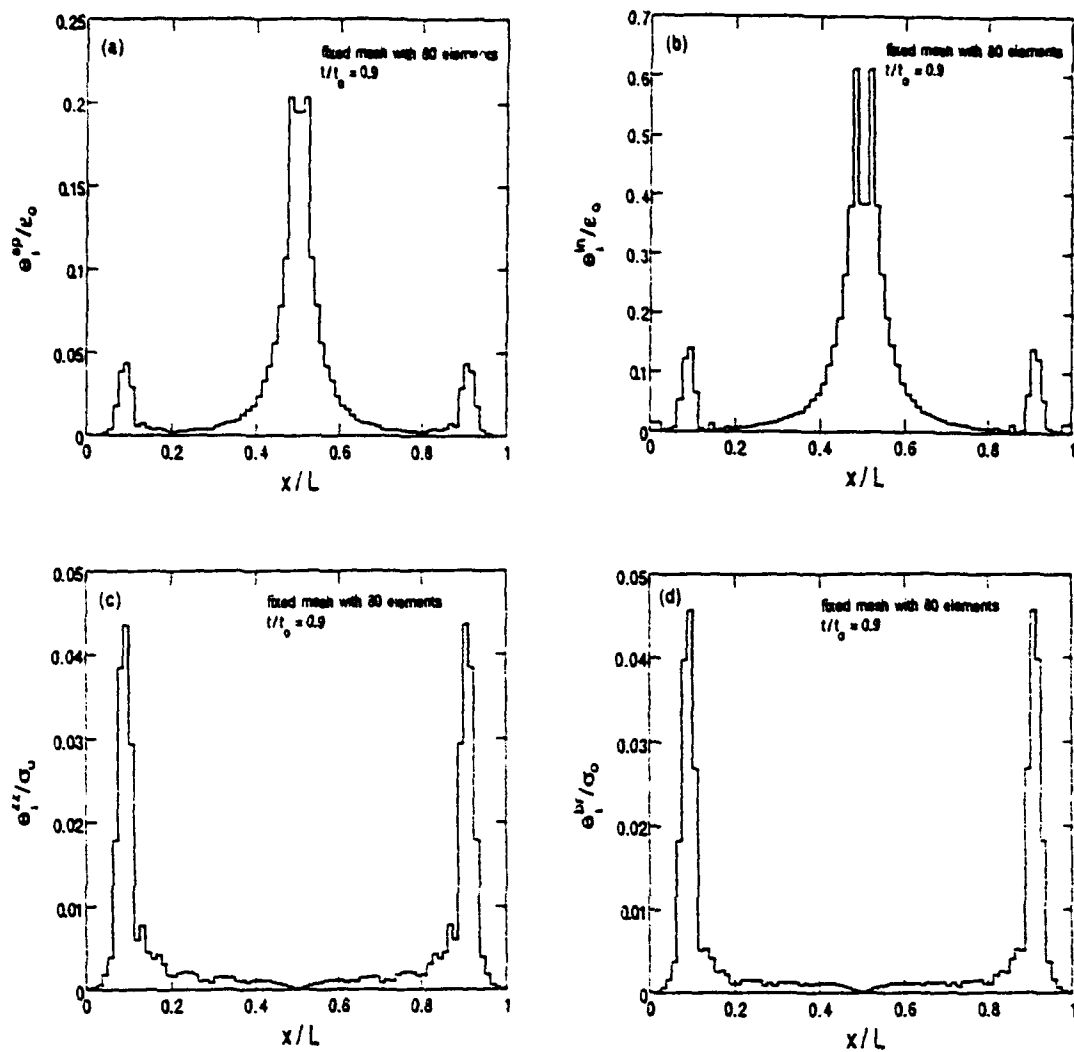


Fig. 2.5. Error profiles for one dimensional localization problem using: (a) strain projection (SP), (b) interpolation (IN), (c) Zienkiewicz-Zhu (ZZ), and (d) Babuska-Rheinboldt (BR)

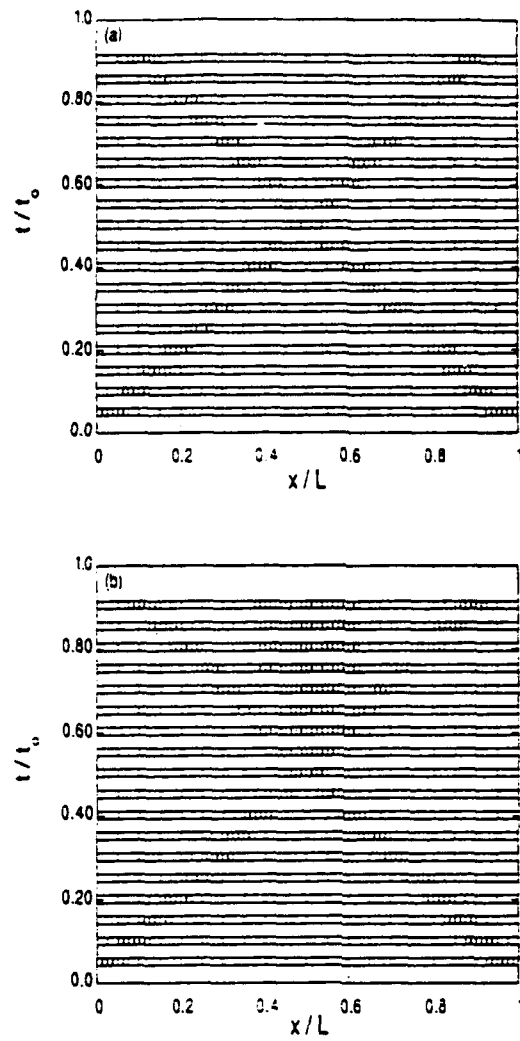


Fig. 2.6. Evolution of mesh with time guided by (a) Zienkiewicz-Zhu (b) strain-projection error measures

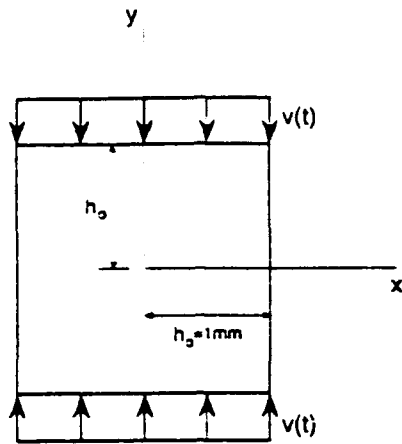


Fig. 2.7. Block subjected to compression

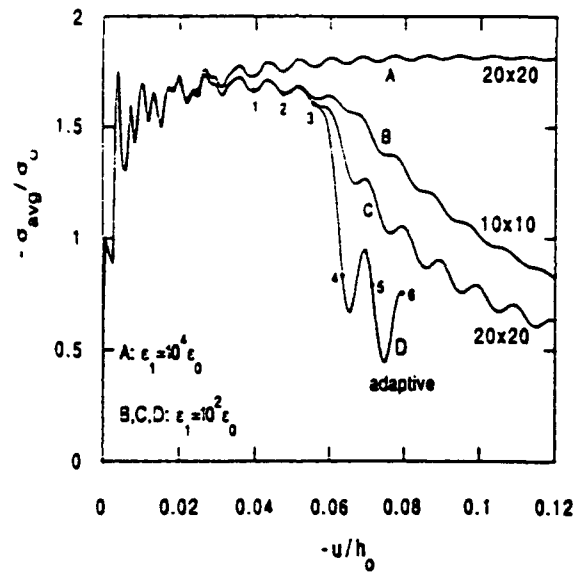


Fig. 2.8. Average stress versus end displacement curves for the block in Figure 7 using a hardening material (curve A) and a softening material (curves B, C, D)

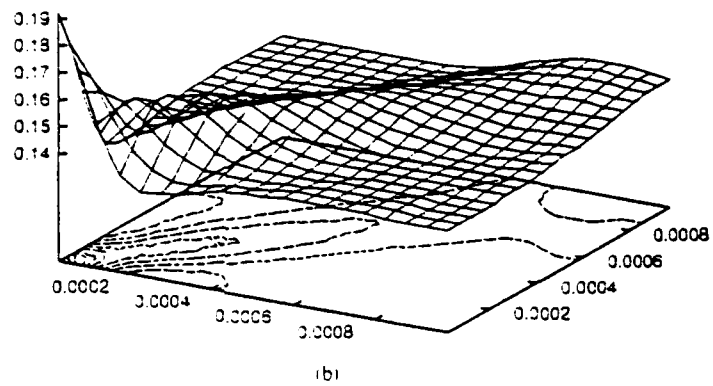
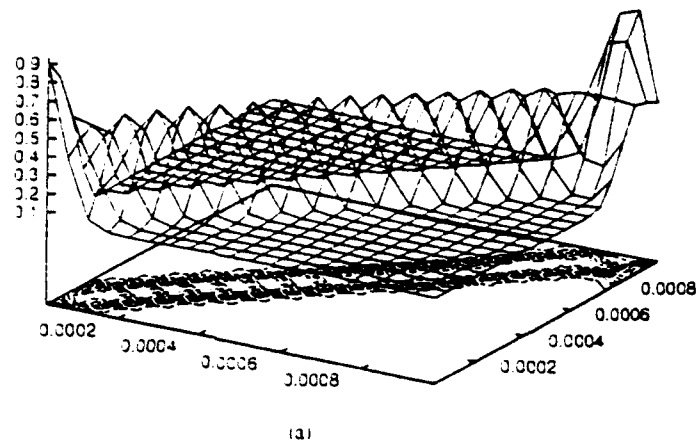


Fig. 2.9. Effective strain surfaces at $-u \cdot h_0 = 0.12$ corresponding to (a) curve C and (b) curve A in Figure 2.8.

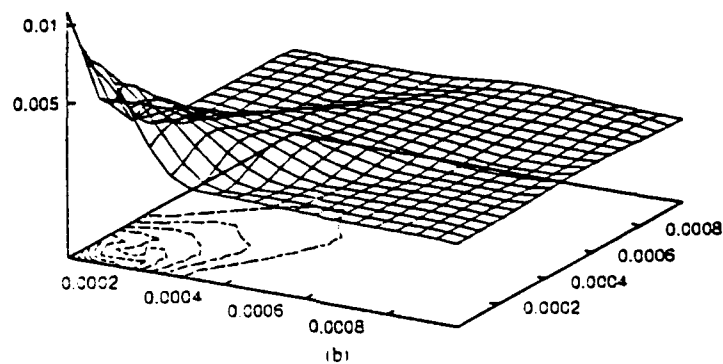
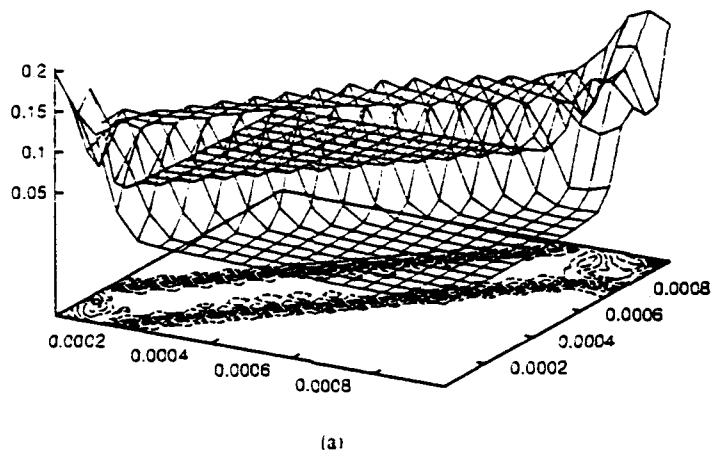


Fig. 2.10. Strain-projection error surfaces at $-u \cdot h_0 = 0.12$ corresponding to (a) curve C and (b) curve A in Figure 2.8.

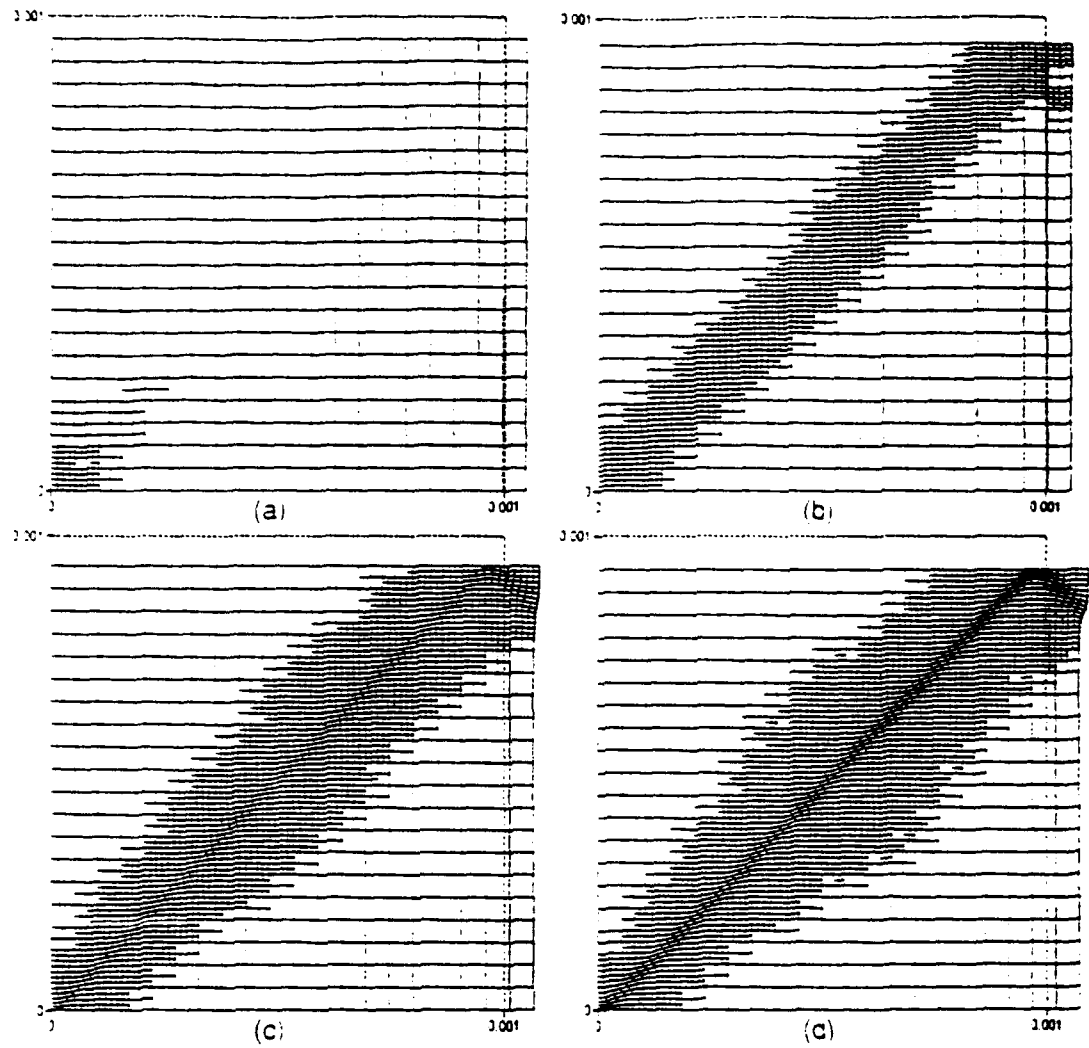


Fig. 2.11. Adaptive mesh evolution corresponding to curve D in Figure 2.8.

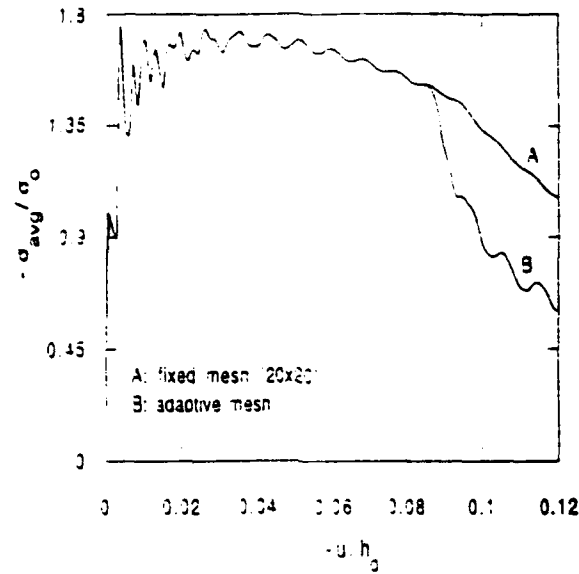


Fig. 2.12. Average stress versus end displacement curves for a softening material with no imperfection

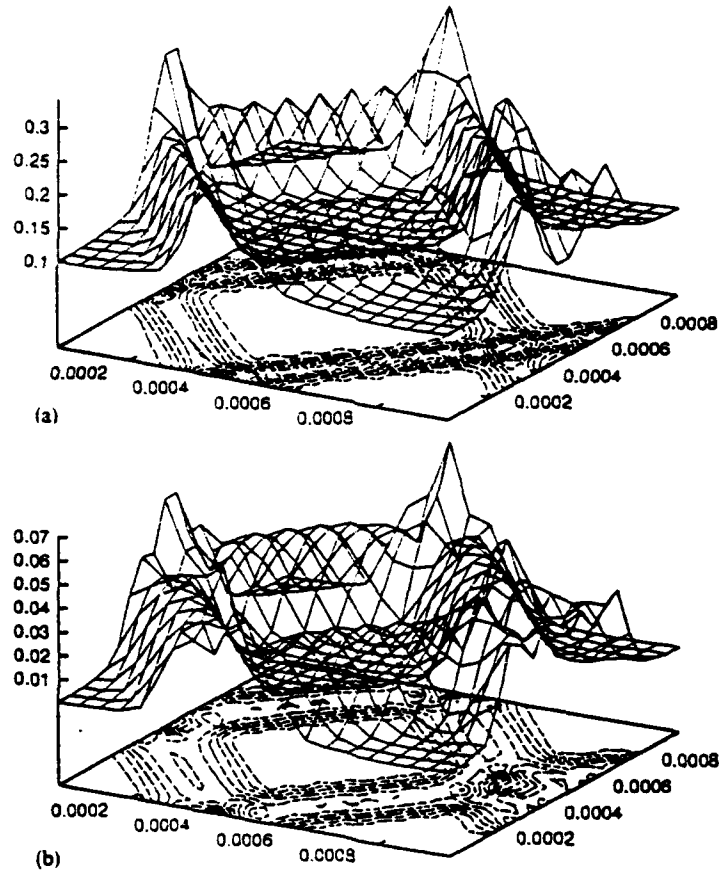


Fig. 2.13. (a) Effective strain and (b) strain-projection error surfaces corresponding to curve A (Figure 12) at $-u/h_0 = 0.12$

0.001

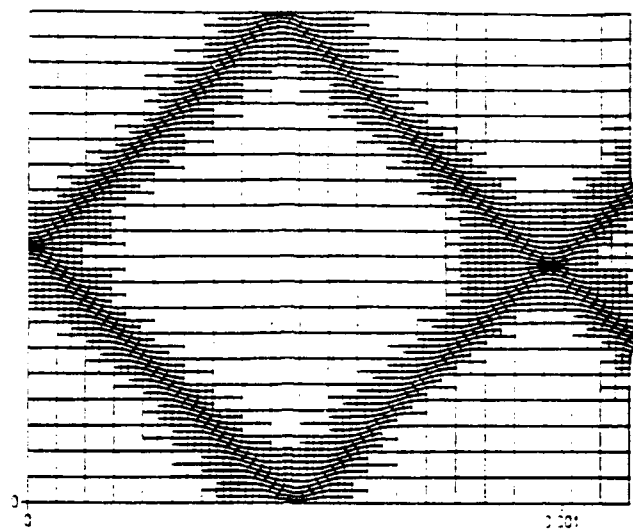


Fig. 2.14. Adaptive mesh corresponding to curve B Fig. 2.12.

0.001

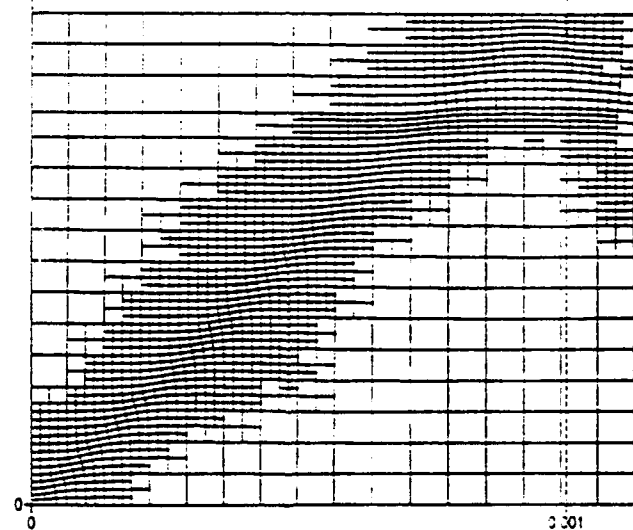


Fig. 2.15 (a). Adaptive mesh

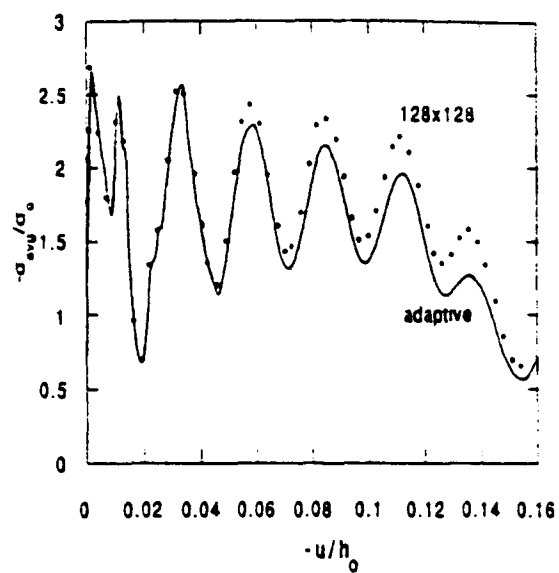


Fig. 2.15 (b). Average stress versus end displacement curve for a softening solid

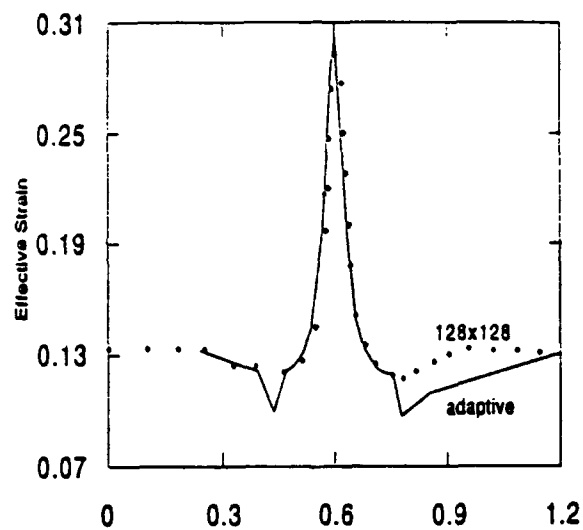


Fig. 2.15 (c). Effective strain across the shear band along the normal direction